Energy, Mines and Resources Canada | Énergie, Mines et Ressources Canada

CANMET

Canada Centre for Mineral and Energy Technology | Centre canadien de la technologie des minéraux et de l'énergie

HIGH TEMPERATURE AND PRESSURE TRIAXIAL COMPRESSION TESTS ON SAMPLE FROM BOREHOLE URL-6

R. Jackson
Rock Mechanics Laboratory

MARCH 1984

ENERGY RESEARCH PROGRAM
MINING RESEARCH LABORATORIES
DIVISION REPORT ERP/MRL 84-22(TR)

58pp

This document ... interim report ... the opinions of ... for Mineral and the ... (CANMET)

... rapport ... rédigé ... de ... ces opinions ... relative de ... canadien de ... minéraux et de ... (CANMET)

DEC 1 0 1984

MICROMEDIA

CONTENTS

	Page
INTRODUCTION	1
CHANGES IN PROCEDURE	1
Ambient strain gauge configuration	1
High temperature strain gauge configuration	2
CHANGES IN ANALYSIS	2
DATA SUMMARY	3
FAILURE CHARACTERISTICS	3
EFFECT OF CONFINING PRESSURE AND TEMPERATURE ON TRIAXIAL STRENGTH	4
EFFECT OF CONFINING PRESSURE AND TEMPERATURE ON THE TANGENT MODULUS OF ELASTICITY	7
EFFECT OF TEMPERATURE ON COHESIVE STRENGTH AND ANGLE OF INTERNAL FRICTION	8
REFERENCES	9
APPENDIX A	A-23

TABLES

No.		
1.	Results of triaxial tests on URL 6 specimens	4
2.	Comparison of predicted and actual failure angles	6
3.	Triaxial strengths normalized to 21°C and 3.5 MPa confining pressure	7

FIGURES

No.		
1.	High temperature strain gauge configuration	10
2.	Mohr's circle and strength envelope: URL-6, 21°C	11
3.	Mohr's circle and strength envelope: URL-6, 100°C	12
4.	Mohr's circle and strength envelope: URL-6, 200°C	13
5.	Deviatorial stress vs confining pressure: URL-6 224 - 260 m horizon, 21°C	14

Figures (Cont'd)

		Page
6.	Deviatorial stress vs confining pressure: URL-6 224 - 260 m horizon, 21°C	15
7.	Deviatorial stress vs confining pressure: URL-6 224 - 260 m horizon, 100°C	16
8.	Deviatorial stress vs confining pressure: URL-6 224 - 260 m horizon, 200°C	17
9.	Deviatorial stress vs temperature: URL-6 224 - 260 m horizon,	18
10.	Tangent modulus of elasticity vs confining pressure: URL-6 224 - 260 m horizon, 21°C	19
11.	Tangent modulus of elasticity vs confining pressure: URL-6 224 - 260 m horizon, 100°C	19
12.	Tangent modulus of elasticity vs confining pressure: URL-6 224 - 260 m horizon, 200°C	19
13.	Tangent modulus of elasticity vs temperature: URL-6 224 - 260 m horizon, 3.5 MPa	20
14.	Tangent modulus of elasticity vs temperature: URL-6 224 - 260 m horizon, 10.0 MPa	20
15.	Tangent modulus of elasticity vs temperature: URL-6 224 - 260 m horizon, 17.0 MPa	20
16.	Tangent modulus of elasticity vs temperature: URL-6 224 - 260 m horizon, 26.0 MPa	21
17.	Tangent modulus of elasticity vs temperature: URL-6 224 - 260 m horizon, 35.0 Mpa	21
18.	Cohesive strength vs temperature: URL-6 224 - 260 m horizon	22
19.	Angle of internal friction vs temperature: URL-6 224 - 260 m horizon	22
A1.	Deviatorial stress vs strain: URL-6 224.50 (3.5 MPa)	A-24
A2.	Deviatorial stress vs strain: URL-6 256.67 (3.5 MPa)	A-25
A3.	Deviatorial stress vs strain: URL-6 224.62 (10.0 MPa)	A-26
A4.	Deviatorial stress vs strain: URL-6 257.60 (10.0 MPa)	A-27
A5.	Deviatorial stress vs strain: URL-6 224.74 (17.0 MPa)	A-28
A6.	Deviatorial stress vs strain: URL-6 257.72 (17.0 MPa)	A-29

Figures (Cont'd)

	Page
A7. Deviatorial stress vs strain: URL-6 225.50 (26.0 MPa)	A-30
A8. Deviatorial stress vs strain: URL-6 257.84 (26.0 MPa)	A-31
A9. Deviatorial stress vs strain: URL-6 224.90 (35.0 MPa)	A-32
A10. Deviatorial stress vs strain: URL-6 258.08 (35.0 MPa)	A-33
A11. Deviatorial stress vs strain: URL-6 226.25 (3.5 MPa)	A-34
A12. Deviatorial stress vs strain: URL-6 256.51 (3.5 MPa)	A-35
A13. Deviatorial stress vs strain: URL-6 225.74 (10.0 MPa)	A-36
A14. Deviatorial stress vs strain: URL-6 258.20 (10.0 MPa)	A-37
A15. Deviatorial stress vs strain: URL-6 225.62 (17.0 MPa)	A-38
A16. Deviatorial stress vs strain: URL-6 258.46 (17.0 MPa)	A-39
A17. Deviatorial stress vs strain: URL-6 225.90 (26.0 MPa)	A-40
A18. Deviatorial stress vs strain: URL-6 258.82 (26.0 MPa)	A-41
A19. Deviatorial stress vs strain: URL-6 226.02 (35.0 MPa)	A-42
A20. Deviatorial stress vs strain: URL-6 258.70 (35.0 MPa)	A-43
A21. Deviatorial stress vs strain: URL-6 226.37 (3.5 MPa)	A-44
A22. Deviatorial stress vs strain: URL-6 227.42 (3.5 MPa)	A-45
A23. Deviatorial stress vs strain: URL-6 228.45 (3.5 MPa)	A-46
A24. Deviatorial stress vs strain: URL-6 226.60 (10.0 MPa)	A-47
A25. Deviatorial stress vs strain: URL-6 228.33 (10.0 MPa)	A-48
A26. Deviatorial stress vs strain: URL-6 226.72 (17.0 MPa)	A-49
A27. Deviatorial stress vs strain: URL-6 259.26 (17.0 MPa)	A-50
A28. Deviatorial stress vs strain: URL-6 227.30 (26.0 MPa)	A-51
A29. Deviatorial stress vs strain: URL-6 228.18 (26.0 MPa)	A-52
A30. Deviatorial stress vs strain: URL-6 225.10 (35.0 MPa)	A-53
A31. Deviatorial stress vs strain: URL-6 226.94 (35.0 MPa)	A-54

INTRODUCTION

High temperature and pressure triaxial testing was conducted on samples obtained from borehole URL-6 in the Lac du Bonnet plutonic formation. Samples originated from a depth of 224 m to 260 m and are generally described as granitic. A more complete geological description may be found in Wong et al. (1).

The testing procedure and methods of data analysis outlined in CANMET Division Report ERP/MRL 80-102(TR) have been modified somewhat for this program (2). The purpose of this report is to briefly describe the procedural changes and present the experimental results. Data analysis and a description of the effects of temperature and confining pressure on triaxial strength, tangent modulus of elasticity, cohesive strength and angle of internal friction are also presented.

CHANGES IN PROCEDURE

Previous high temperature and pressure testing programs have employed linear variable differential transducers attached to the triaxial cell and loading head to measure sample deformation. Recently, an effort has been made to achieve more accurate and repeatable measurements of axial deformation by using electrical resistance type strain gauges mounted directly on the copper specimen jacket. The viability and accuracy of this method was verified by testing a steel 'dummy' of known deformational properties under the various test conditions. Based on the calibration data, it became necessary to employ two different gauge configurations for ambient and high temperature conditions.

Ambient Strain Gauge Configuration

As ambient testing implies, the temperature both in and outside the test chamber is nearly equal. This enabled us to utilize two conventional half bridge strain gauge configurations with the dummy sides of the bridges located external to the chamber. Two measuring circuits were used to guard against the failure of any one of the gauges during testing.

The bridges were hooked up to two Bruel and Kjaer Type 1526 strain indicators which were in turn connected to a Fluke 2240 data logger and a Hewlett Packard 7046B X-Y recorder. The data logger was used to record the

strain measurements, confining pressure, and load and cnamber temperature profile at ten second intervals during testing; while the X-Y recorder provided continuous monitoring of load versus displacement.

High Temperature Strain Gauge Configuration

The high temperature environment caused several problems in attempting to use gauges to measure axial deformation. It was especially desireable to have two independent measuring circuits during testing at elevated temperatures, as equipment failure after heating would render a specimen useless. It was also necessary to have the dummy side of the bridge at the same temperature as the active gauges to prevent undue instrument drift during the heating cycle. Unfortunately, the loading piston was only equipped with four electrical feed throughs. This necessitated the development of the special bridge configuration seen in Fig. 1. Dummy gauges were mounted on a steel collar which was attached to the bottom sealing platen with set screws.

The measuring circuit was connected to a B&F Instruments ICI613 input conditioner and PS15-1500 power supply. These, in turn, were hooked up to the data logger and X-Y recorder and readings were taken as before.

CHANGES IN ANALYSIS

During previous testing programs, data was reduced manually and the resulting stress/strain curve plotted by hand. This curve was then used to determine the tangent modulus of elasticity by drawing in the tangent at 50% of the failure load and calculating the slope of the line. While this procedure proved adequate, it was time consuming and open to a degree of subjectivity from experimenter to experimenter.

For this program, the data was loaded from the data logger to a VAX 750 computer which in turn reduced and plotted the resulting stress/strain points. A third degree equation of the form;

$$\text{stress} = A*\text{strain} + B*\text{strain}^2 + C*\text{strain}^3 \qquad (1)$$

was fitted to these points. The strain at 50% of the failure load was interpolated between the appropriate points contained in the output and this value was substituted into the first derivative of Equation 1. The tangent modulus was then calculated according to the equation;

$$\text{stress} = A + 2B*\text{strain} + 3C*\text{strain}^2 \qquad (2)$$

(where, A, B and C are regressed constants)

The method was verified by first reducing all the ambient temperature tests as before and calculating the modulus by hand. The data was then fed into the computer and the results were compared. The average difference between the two methods was 1.38 GPa with a difference of less than 1 GPa for six of the ten tests.

DATA SUMMARY

Table 1 summarizes the specimen dimensions, test configuration, axial stress rate, deformational properties, triaxial strength and failure characteristics. The computer generated stress/strain curves are contained in Fig. A1 through A32 in Appendix A.

FAILURE CHARACTERISTICS

The predominant mode of failure was a violent brittle fracture along a single diagonal failure plane. Considerable fragmentation occurred and the occasional bottom wedge was noted. It seemed that the degree of axial splitting increased with increasing temperature.

Where single diagonal failure planes resulted, the failure angles ranged from 62° to 76°. The observed mean failure angle was 69.1° with a standard deviation of 3.65° and variance of 12.8°. Mohr-Coulomb analyses were conducted using the 3.5, 17.0 and 35.0 MPa confining pressure results for each of the three temperature ranges (see Fig. 2, 3 and 4). A comparison of observed failure angles and those predicted by the analyses are contained in Table 2. The average difference between the predicted and actual failure angles was 4.0°. It is interesting to note that the variation tends to become larger with increasing temperature.

Table 1 - Results of Triaxial Compression test on URL6 Specimens

Specimen identification	Length (mm)	Diameter (mm)	Confining pressure σ3(MPa)	Temperature (°C)	Axial Stress Rate (MPa/sec)	Total axial Strain(%)	Triaxial Strength (GPa)	Tangent Modulus (GPa)	Fracture Plane Orientation	Failure Characteristics
URL6 224.50	117.65	44.5	3.5	21	0.83	0.4275	280	68.87	76°	Violent brittle fracture single, diagonal failure plane.
URL6 256.67	116.05	44.79	3.5	21	1.02	0.4375	302	68.08	N/A	Violent brittle fracture bottom hedge failure.
URL6 224.62	115.10	44.80	10.0	21	0.77	0.6450	384	68.26	73°	Violent brittle fracture single, diagonal failure plane.
URL6 257.60	117.28	44.55	10.0	21	0.84	0.6000	364	70.86	N/A	Violent brittle fracture partially formed bottom hedge.
URL6 224.74	114.72	44.80	17.0	21	0.77	0.7500	435	66.63	74°	Violent brittle fracture single, diagonal failure plane.
URL6 257.72	115.42	44.52	17.0	21	0.86	0.6950	434	68.69	74°	Violent brittle fracture single, diagonal failure plane.
URL6 225.50	118.65	44.77	26.0	21	0.71	0.9000	507	64.86	N/A	Violent brittle fracture single, diagonal failure plane.
URL6 257.84	113.07	44.51	26.0	21	0.87	0.9300	513	66.21	72°	Violent brittle fracture single, diagonal failure plane.
URL6 224.90	118.81	44.81	35.0	21	0.93	0.9600	552	69.46	71°	Violent brittle fracture single, diagonal failure plane.
URL6 258.08	118.63	44.52	35.0	21	0.98	0.9150	551	70.10	71°	Violent brittle fracture partially developed diagonal failure.
URL6 226.25	116.45	44.74	3.5	100	1.10	0.4526	275	74.67	69°	Violent brittle fracture single, diagonal failure plane.
URL6 256.51	117.15	44.56	3.5	100	1.06	0.5007	278	71.42	69°	Violent brittle fracture partially formed bottom hedge.
URL6 225.74	116.11	44.74	10.0	100	1.08	0.4778	286*	73.40	62°	Violent brittle fracture single, diagonal failure plane.
URL6 258.20	115.91	44.57	10.0	100	1.21	0.5625	335	70.76	N/A	Violent brittle fracture bottom hedge failure.
URL6 225.62	115.33	44.76	17.0	100	0.72	0.6848	421	72.73	69°	Violent brittle fracture single, diagonal failure plane.
URL6 258.46	114.49	44.53	17.0	100	0.81	0.6576	413	76.73	68°	Single, diagonal failure plane. violent brittle fracture
URL6 225.90	116.35	44.75	26.0	100	0.81	0.9400	459	61.91	69°	Violent brittle fracture single, diagonal failure plane

*Values were treated as outliers and not considered in mean calculations

Table 1 (Continued)

Specimen identification	Length (mm)	Diameter (mm)	Confining pressure σ3(MPa)	Temperature (°C)	Axial Stress Rate (MPa/sec)	Total axial Strain(%)	Triaxial Strength (GPa)	Tangent Modulus (GPa)	Fracture Plane Orientation	Failure Characteristics
URL6 228.82	117.21	44.53	26.0	100	0.87	1.0599	496	65.66	65°	Violent brittle fracture bottom hedge failure.
URL6 226.02	115.65	44.77	35.0	100	0.88	0.8999	534	74.44	67°	Violent brittle fracture single, diagonal failure plane.
URL6 258.70	115.80	44.52	35.0	100	0.87	0.8452	536	73.54	69°	Violent brittle fracture partially formed bottom hedge.
URL6 226.37	116.35	44.75	3.5	200	0.78	0.3784	239	63.99	65°	Violent brittle fracture single, diagonal failure plane.
URL6 227.42	116.57	44.76	3.5	200	1.10	0.4165	217	61.22	N/A	Violent brittle fracture single, diagonal failure plane.
URL6 228.45	117.08	44.76	3.5	200	0.81	0.4256	221	61.40	69°	Violent brittle fracture single, diagonal failure plane.
URL6 226.60	116.85	44.72	10.0	200	0.69	0.4234	99	82.87*	N/A	Violent brittle fracture bottom hedge failure.
URL6 228.33	117.76	44.82	10.0	200	0.91	0.5132	330	72.68	75°	Violent brittle fracture single, diagonal failure plane.
URL6 226.72	117.64	44.78	17.0	200	0.73	0.6807	359	68.74	66°	Violent brittle fracture single, diagonal failure plane.
URL6 259.26	116.42	44.56	17.0	200	1.04	0.6808	359	62.84	N/A	Violent brittle fracture bottom hedge failure.
URL6 227.30	115.06	44.78	26.0	200	0.97	0.7501	448	70.11	67°	Violent brittle fracture single, diagonal failure plane.
URL6 228.18	115.64	44.76	26.0	200	0.92	0.6761	460	81.93*	69°	Violent brittle fracture single, diagonal failure plane.
URL6 225.10	117.60	44.78	35.0	200	N/A	0.8525	550	75.85	63°	Violent brittle fracture single, diagonal failure plane.
URL6 226.94	116.03	44.76	35.0	200	0.94	0.9790	501	67.31	67°	Violent brittle fracture single, diagonal failure plane.

*Values were treated as outliers and not considered in mean calculations

Table 2 - Comparison at predicted and actual failure angles

Temperature (°C)	Confining pressure (MPa)	θ predicted	θ actual	Δθ
21	3.5	74.5°	76.0°	+1.5°
	17.0	72.0°	74.0°	+2.0°
			74.0°	+2.0°
	35.0	70.5°	71.0°	+0.5°
			71.0°	+0.5°
100°	3.5	76.0°	69.0°	-7.0°
			69.0°	-7.0°
	7.0	71.5°	69.0°	-2.5°
	35.0	69.0°	67.0°	-2.0°
			69.0°	
200°	3.5	73.5°	65.0°	-8.5°
	17.0	73.0°	66.0°	-8.0°
	35.0	72.5°	67.0°	-5.5°
			63.0°	-9.5°

EFFECT OF CONFINING PRESSURE AND TEMPERATURE ON TRIAXIAL STRENGTH

As expected, the URL-6 specimens showed an increase in strength with confining pressure at all temperature levels. The 21° and 100°C temperature ranges exhibited nearly identical strength increases of 260.5 and 258.5 MPa respectively as the confining pressure was increased from 3.5 to 35.0 MPa. The largest triaxial strength increase of 299.5 MPa, however, was observed for measurements conducted at 200°C.

The rate of strength increase seemed to be greatest from 3.5 to 10.0 MPa for the temperature extremes of 21° and 200°C after which it became fairly constant to 35.0 MPa. At 100°C, the rate seems to taper off throughout the confining pressure range (Fig. 5). Table 3 depicts the normalized strength changes with confining pressure and temperature. Experimental data scatter for the three temperature levels are illustrated in Fig. 6, 7 and 8.

Table 3 - Triaxial strengths normalized to 21°C and 3.5 MPa confining pressure

Confining Pressure	Temperature(°C)		
(MPa)	21	100	200
3.5	1.00	0.95	0.78
10.0	1.28	1.15	1.08
17.0	1.49	1.43	1.23
26.0	1.75	1.64	1.56
35.0	1.90	1.84	1.80

Increasing temperature had the effect of decreasing the triaxial strength for all confining pressures tested. The largest decrease (75 MPa) was observed when heating from ambient (21°C) to 200°C at a confining pressure of 17.0 MPa. The confining pressure level least affected by increasing temperature was the 35.0 MPa; a 26 MPa reduction in strength was observed at this confining pressure. Strength decreases of 65, 60 and 56 MPa were observed for confining pressures of 3.5, 10.0 and 26.0 MPa, respectively, when the temperature was increased from 21° to 200°C (Fig. 9).

EFFECT OF CONFINING PRESSURE AND TEMPERATURE ON THE TANGENT MODULUS OF ELASTICITY

The tangent modulus of elasticity measured at 21°C exhibited very little variation with increasing confining pressure. The largest effect was observed at a confining pressure of 26.0 MPa at which the modulus dropped to an average value of 65.53 GPa. The moduli determined for the remaining confining pressures were tightly banded, ranging from an average 67.66 to 69.78 GPa (Fig. 10).

The moduli determined at the 100°C temperature level were, on average, slightly higher than those observed at 21°C. At confining pressures of 3.5, 10.0, 17.0 and 35.0 MPa, the average moduli were 73.04, 72.08, 74.73 and 73.99 GPa, respectively. Tests conducted at 26.0 MPa confining pressure, however, again showed a decrease on modulus where an average value of 63.78 GPa was determined (Fig. 11).

Moduli determined at 200°C showed considerable data scatter and variation between confining pressures. With the exception of the 10.0 MPa confining pressure results, the modulus exhibited fairly regular increases with confining pressure. Values observed at confining pressures of 3.5, 17.0 26.0 and 35.0 MPa were 62.20, 65.79, 70.11 and 71.58 GPa respectively. The highest modulus of 72.68 GPa, however, was determined at the 10.0 MPa confining pressure (Fig. 12).

A similar modulus behaviour was noted for the constant confining pressures of 3.5, 17.0 and 35.0 MPa with increasing temperature. At a confining pressure of 3.5 MPa, the modulus increased by 7% from 21° to 100°C and decreased by 15% from 100° to 200°C. The 17.0 and 35.0 MPa confining pressure results exhibited increases of 10% and 6% and decreases of 12% and 3%, respectively, over the same temperature ranges. Measurements taken at a confining pressure of 10.0 indicated constant increases in modulus of 4% and 1% from 21° to 100°C and 100° to 200°C, respectively. Tests conducted at 26.0 MPa confining pressure showed a decrease in modulus of 3% from 21° to 100°C and an increase of 10% from 100° to 200°C (Fig. 13, 14, 15, 16 and 17).

EFFECT OF TEMPERATURE ON COHESIVE STRENGTH AND ANGLE OF INTERNAL FRICTION

The cohesive strength determined for the confining pressures of 3.5, 17.0 and 35.0 MPa used in the Mohr-Coulomb analyses were all insensitive to increasing temperature with values of 28, 47 and 64 MPa, respectively, for both the 21° and 100°C temperature levels. While the cohesion exhibited at the 3.5 MPa confining pressure continued to remain constant, those observed for 17.0 and 35.0 MPa confining pressures showed significant decreases of 17 and 29 MPa in cohesive strength when the temperature was increased from 100° to 200°C (Fig. 18).

At a constant confining pressure of 3.5 MPa, the angle of internal friction increased by 5% on heating from 21° to 100°C. Subsequent heating to 200°C resulted in a decrease of 8%. Measurements taken at 17.0 MPa exhibited the least sensitivity in terms of the internal friction angle, decreasing by 0.5% from 21° to 100°C. The friction angle determined at 35.0 MPa confining pressure decreased by 6%. Further heating to 200°C resulted in a substantial increase of 16% (Fig. 19).

REFERENCES

1. Wong, A.S. "Modal analyses of URL-1, UR1-2, URL-5, and URL-6 extended engineering core samples from the underground research laboratory site near Lac du Bonnet, Manitoba"; in preparation.

2. Annor, A., Miles P., Kapeller, F. and Larocque, G. "High temperature and pressure triaxial compression tests on rock samples from Pinawa and Creighton Mines"; Technical Report ERP/MRL 80-102 (TR) .

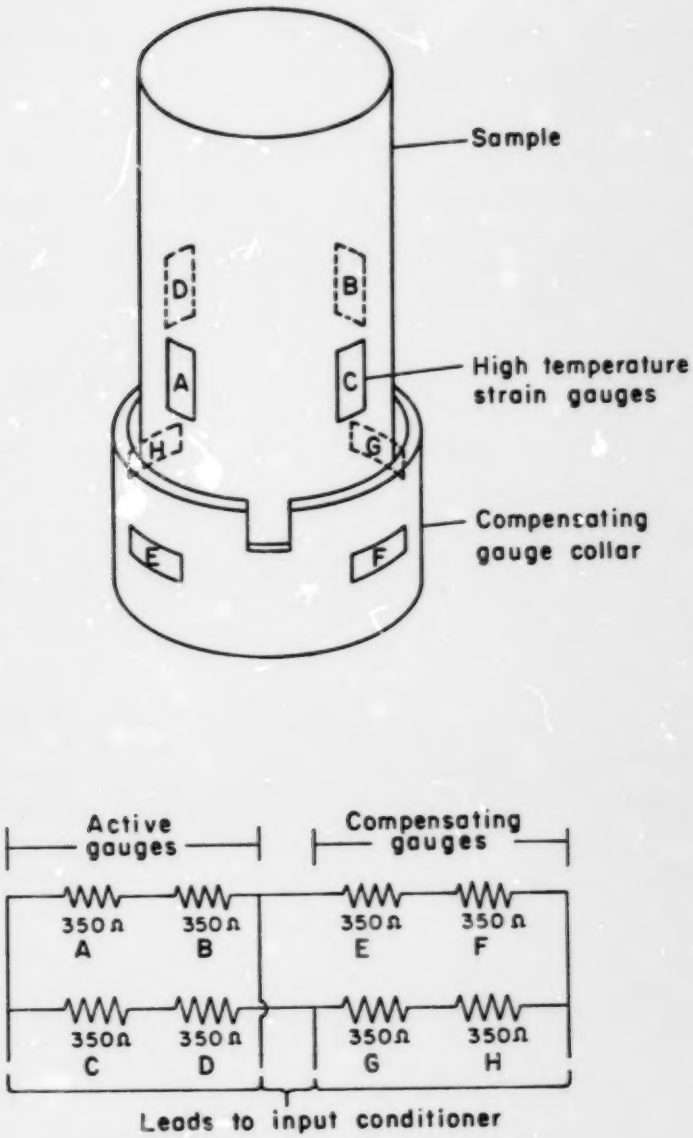

Fig. 1 - High temperature strain gauge configuation

Confining pressure σ_3 (MPa)	Internal friction angle ϕ	Cohesion C (MPa)	Failure plane angle θ	Failure plane stresses (MPa)	
				σ_θ	τ_θ
3.5	$\phi_1 = 59.0°$	$C_1 = 28$	$\theta_1 = 74.5°$	24	75
17.0	$\phi_2 = 54.0°$	$C_2 = 47$	$\theta_2 = 72.0°$	58	128
35.0	$\phi_3 = 51.0°$	$C_3 = 64$	$\theta_3 = 70.5°$	96	174

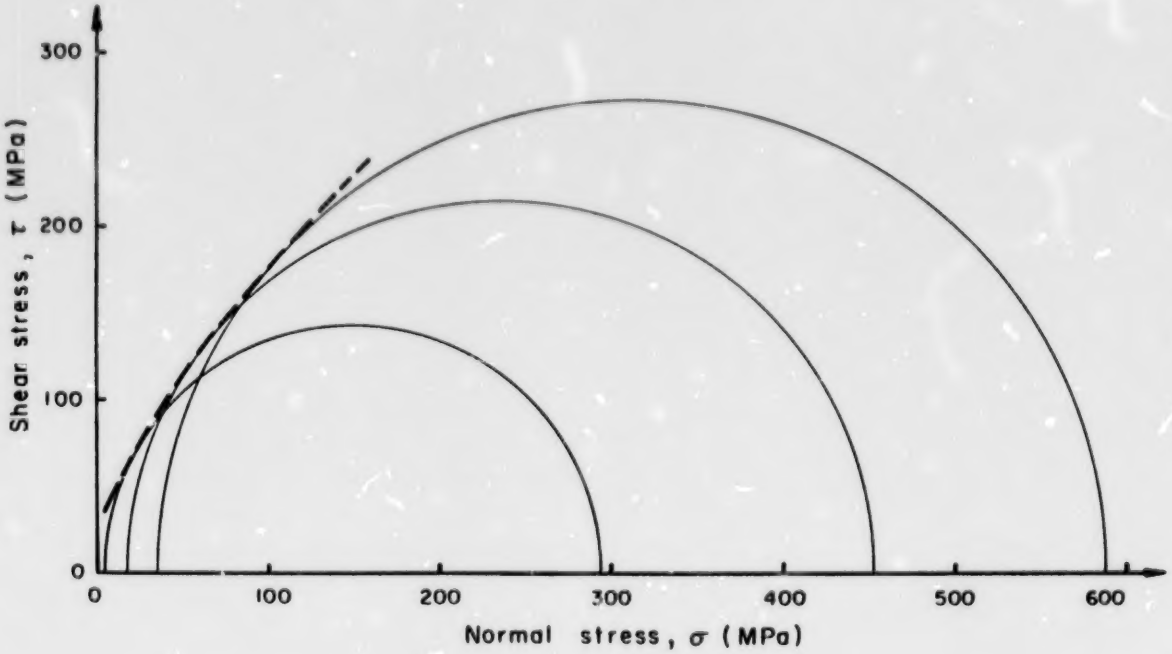

Fig. 2 - Mohr's circle and strength envelope: URL-6, 21°C

Confining pressure σ_3 (MPa)	Internal friction angle ϕ	Cohesion C (MPa)	Failure plane angle θ	Failure plane stresses (MPa)	
				σ_θ	τ_θ
3.5	$\phi_1 = 62.0°$	$C_1 = 28$	$\theta_1 = 76.0°$	20	65
17.0	$\phi_2 = 53.0°$	$C_2 = 47$	$\theta_2 = 71.5°$	59	125
35.0	$\phi_3 = 48.0°$	$C_3 = 64$	$\theta_3 = 69.0°$	104	179

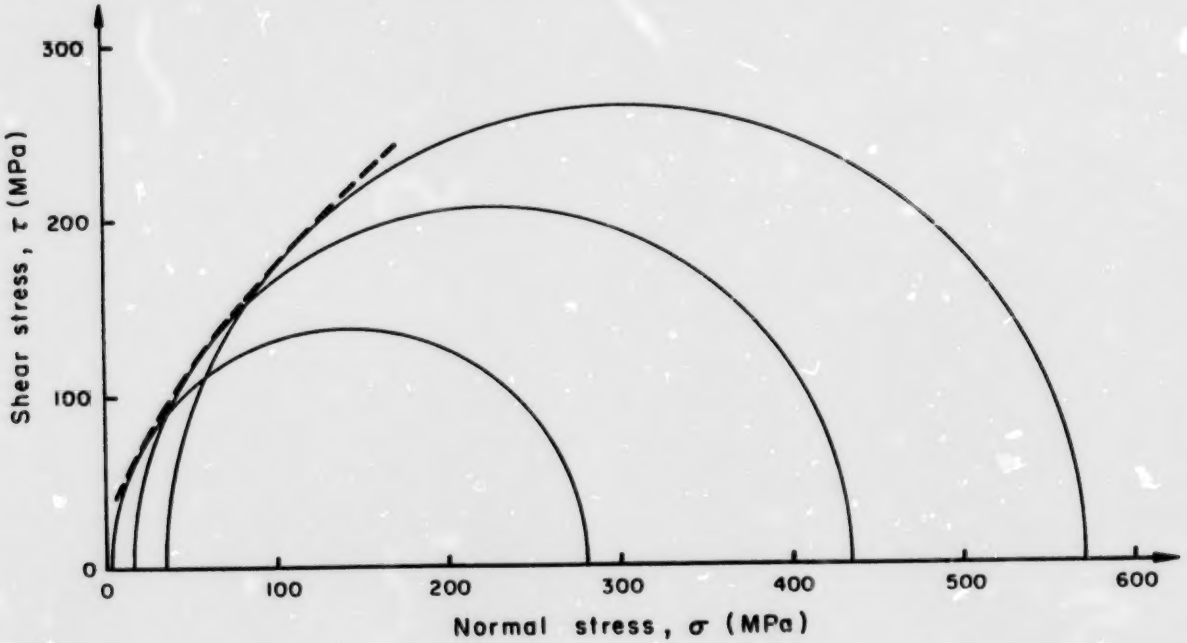

Fig. 3 - Mohr's circle and strength envelope: URL-6, 100°C

Confining pressure σ_3 (MPa)	Internal friction angle ϕ	Cohesion c (MPa)	Failure plane angle θ	Failure plane stresses (MPa)	
				σ_θ	τ_θ
3.5	$\phi_1 = 57.0°$	$C_1 = 28$	$\theta_1 = 73.5°$	22	62
17.0	$\phi_2 = 56.0°$	$C_2 = 30$	$\theta_2 = 73.0°$	48	100
35.0	$\phi_3 = 55.0°$	$C_3 = 35$	$\theta_3 = 72.5°$	82	151

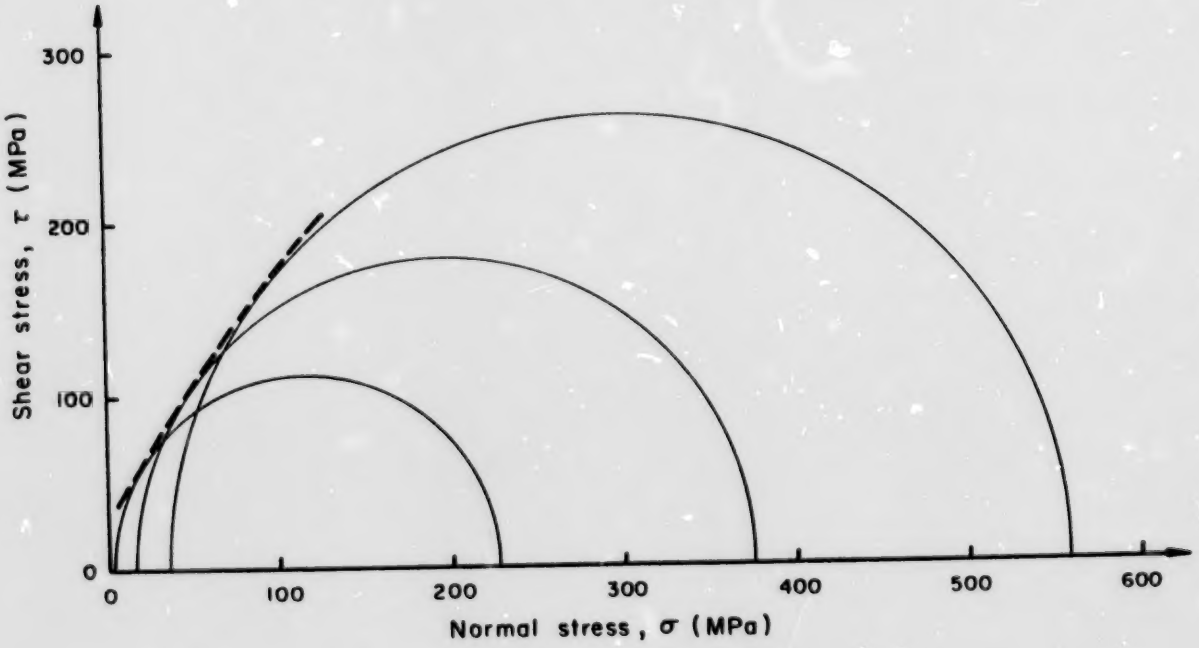

Fig. 4 - Mohr's circle and strength envelope: URL-6, 200°C

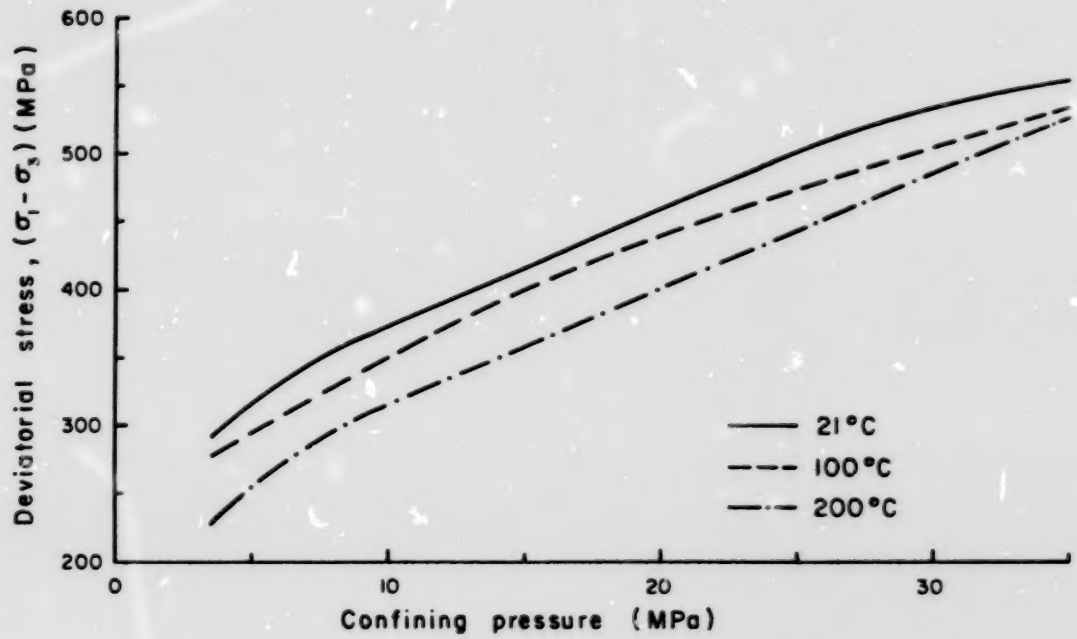

Fig. 5 - Deviatorial stress vs confining pressure: URL-6 224 - 260 m horizon

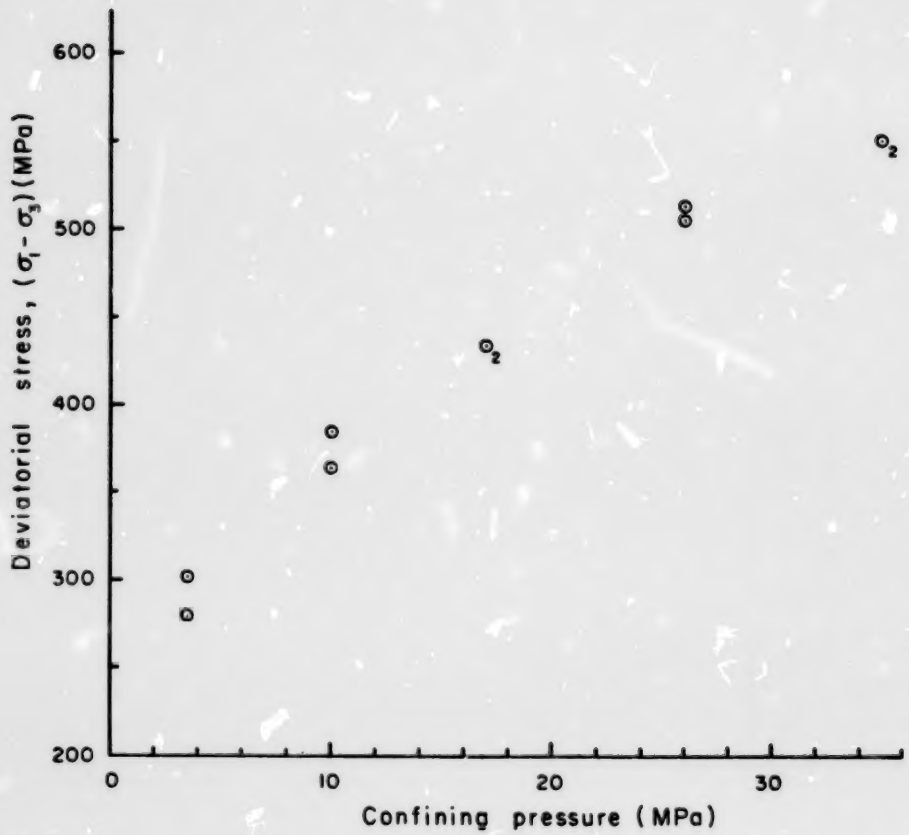

Fig. 6 - Deviatorial stress vs confining pressure: URL-6 224 - 260 m horizon, 21°C

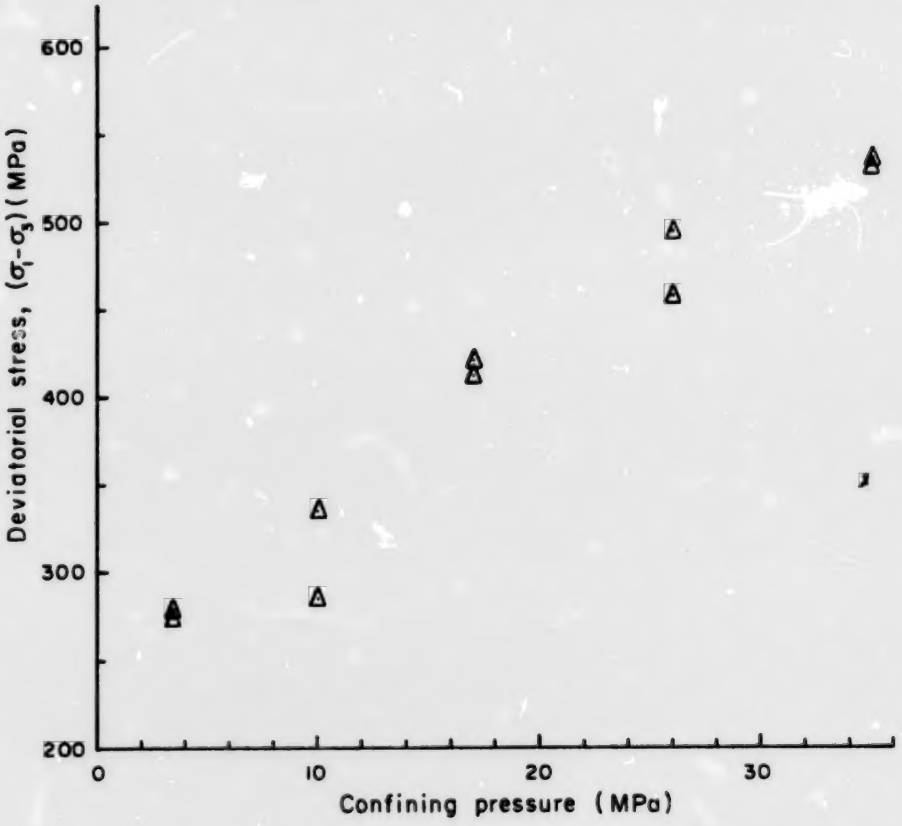

Fig. 7 Deviatorial stress vs confining pressure: URL-6 224 - 260 m horizon, 100°C

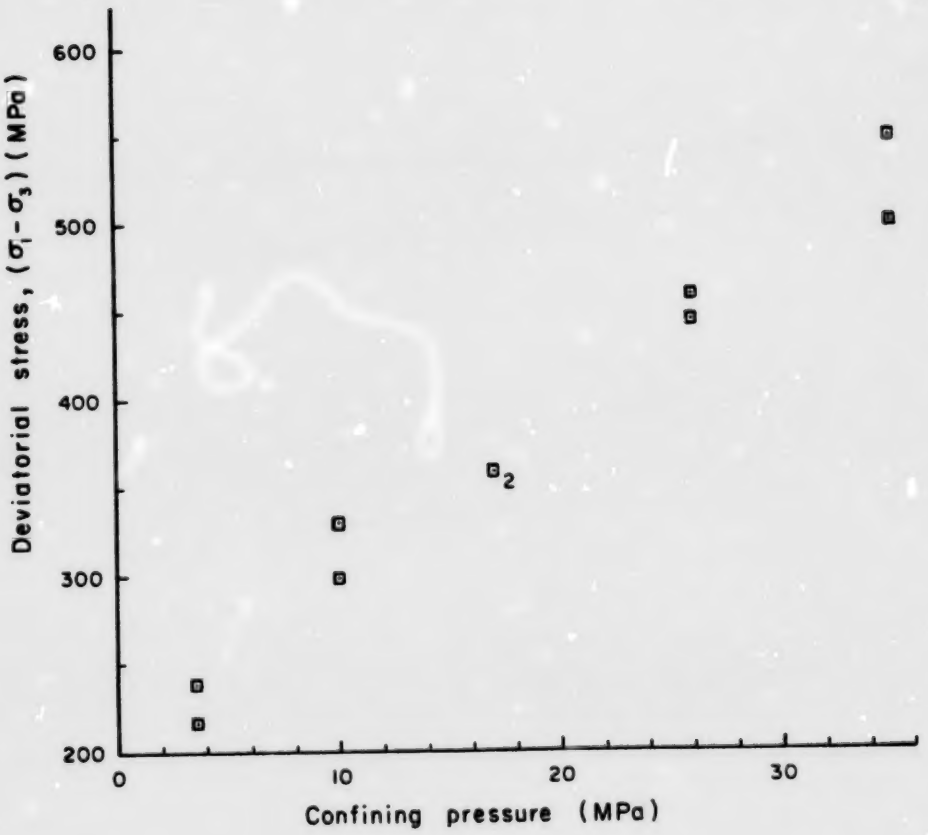

Fig. 8 - Deviatorial stress vs confining pressure: URL-6 224 - 260 m horizon, 200°C

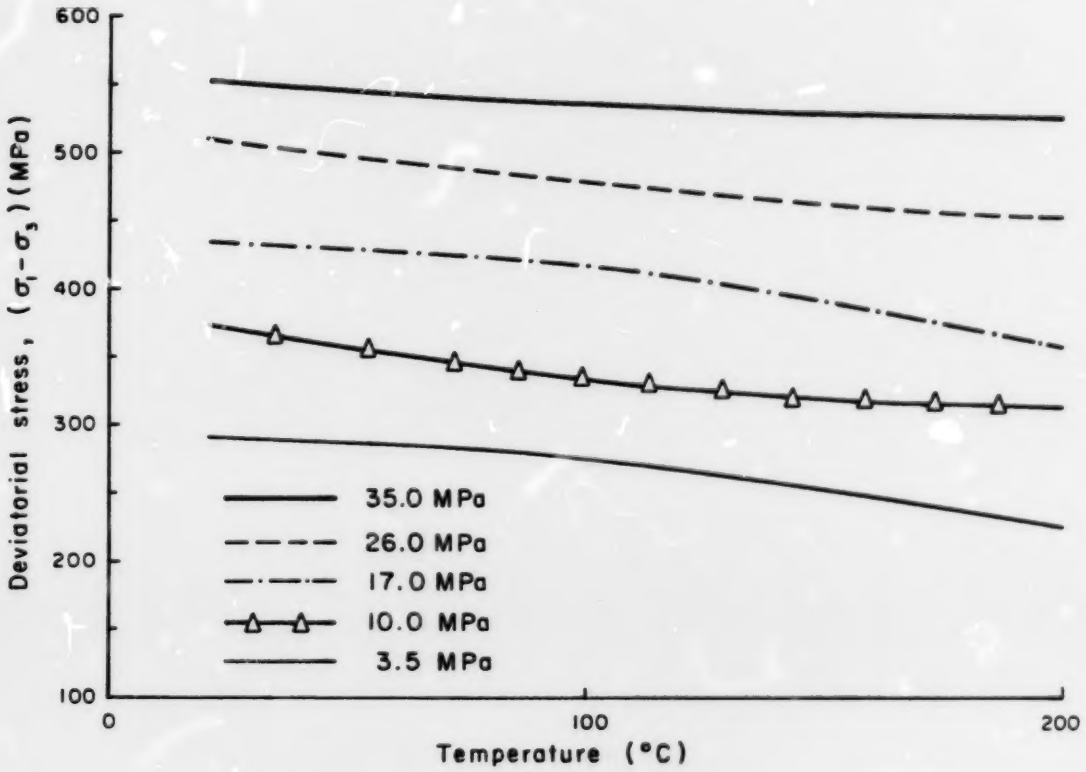

Fig. 9 - Deviatorial stress vs temperature: URL-6 224 - 260 m horizon

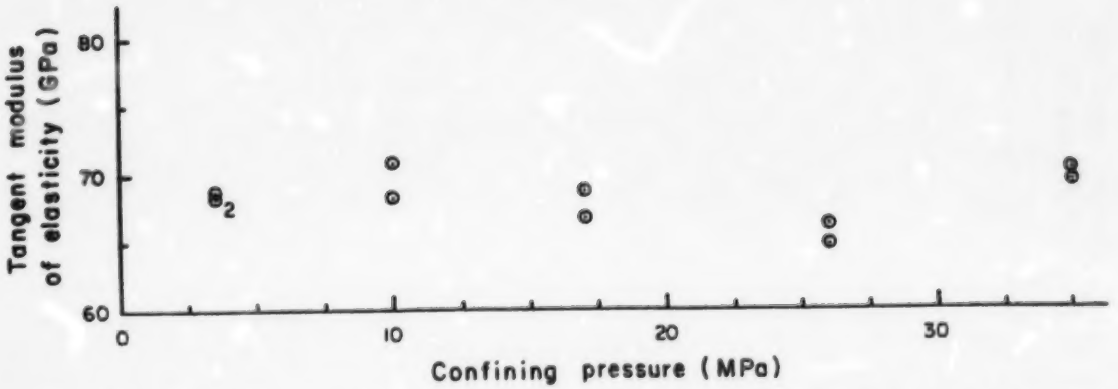

Fig. 10 - Tangent modulus of elasticity vs confining pressure: URL-6 224 - 260 m horizon, 21°C

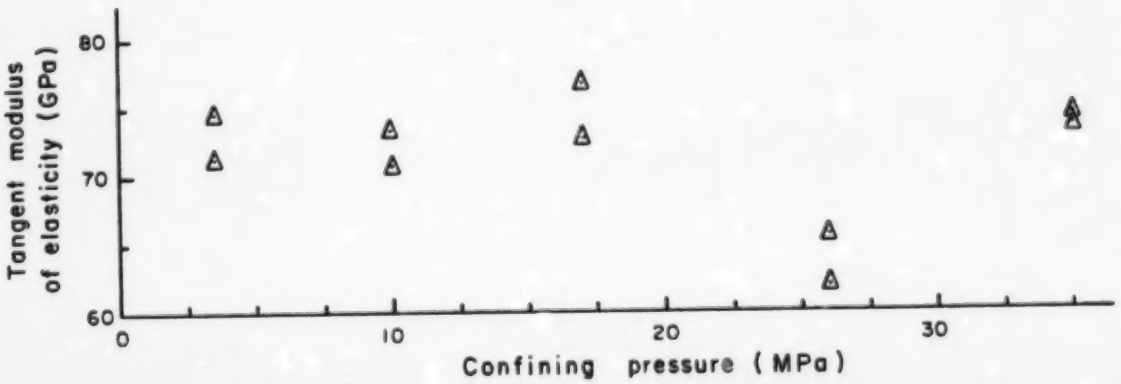

Fig. 11 - Tangent modulus of elasticity vs confining pressure: URL-6 224 - 260 m horizon, 100°C

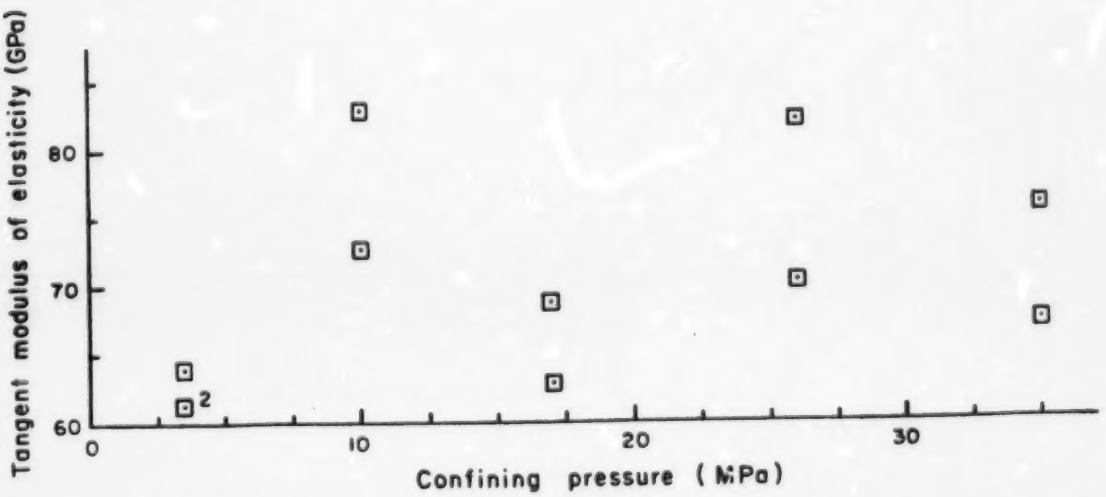

Fig. 12 - Tangent modulus of elasticity vs confining pressure: URL-6 224 - 260 m horizon, 200°C

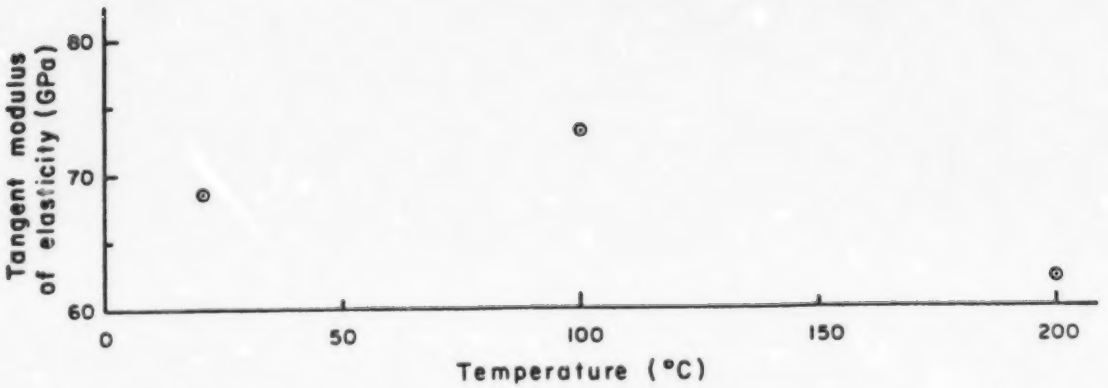

Fig. 13 - Tangent modulus of elasticity vs temperature:
URL-6 224 - 260 m horizon, 3.5 MPa

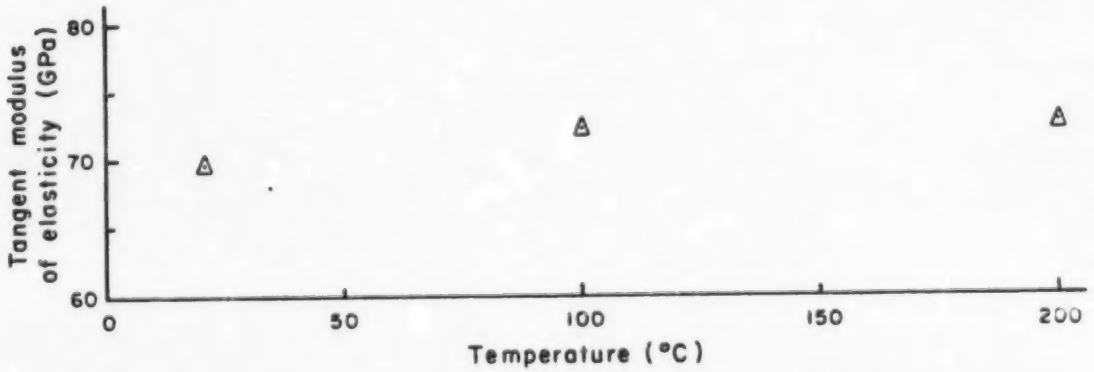

Fig. 14 - Tangent modulus of elasticity vs temperature:
URL-6 224 - 260 m horizon, 10.0 MPa

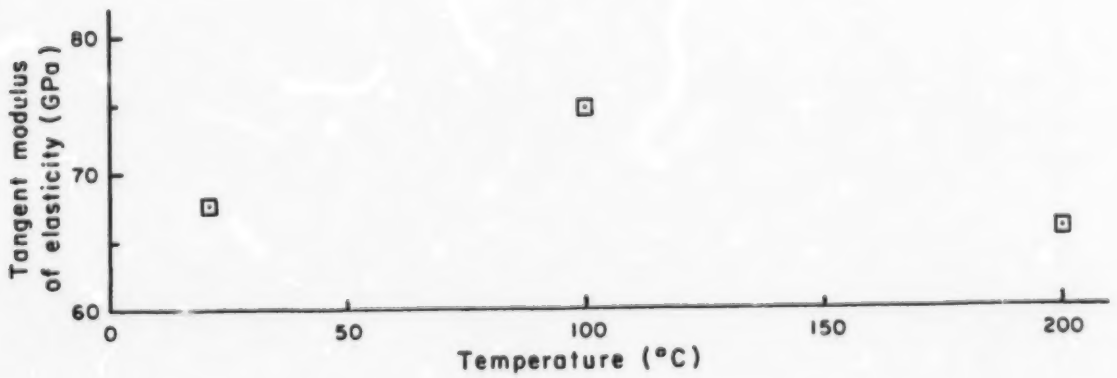

Fig. 15 - Tangent modulus of elasticity vs temperature:
URL-6 224 - 260 m horizon, 17.0 MPa

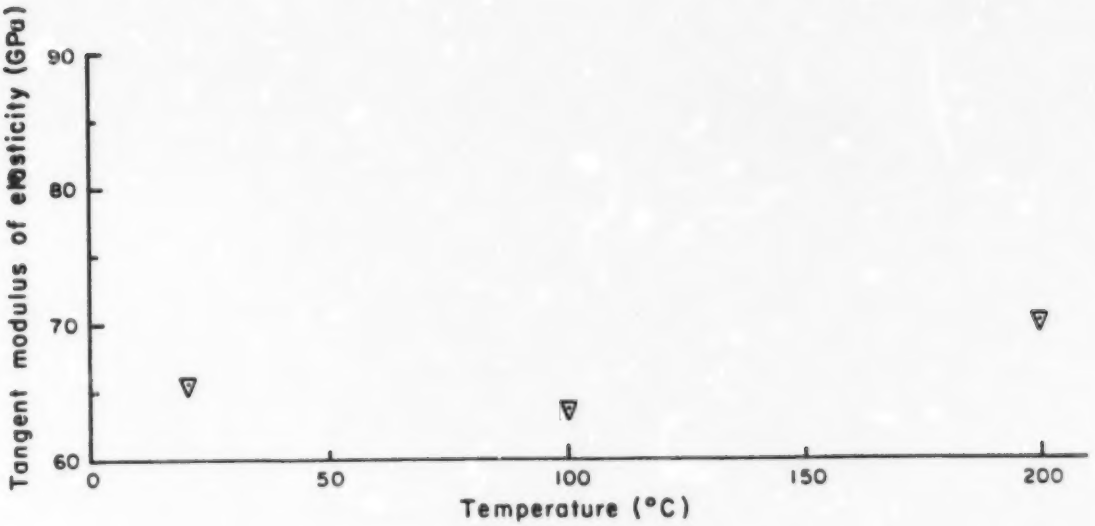

Fig. 16 - Tangent modulus of elasticity vs temperature:
URL-6 224 - 260 m horizon, 26.0 MPa

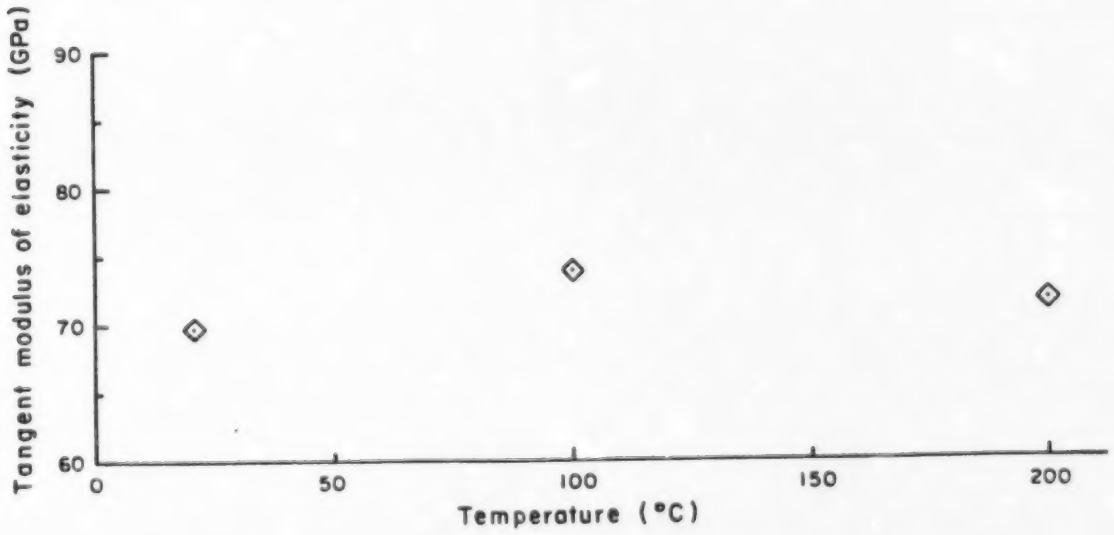

Fig. 17 - Tangent modulus of elasticity vs temperature:
URL-6 224 - 260 m horizon, 35.0 MPa

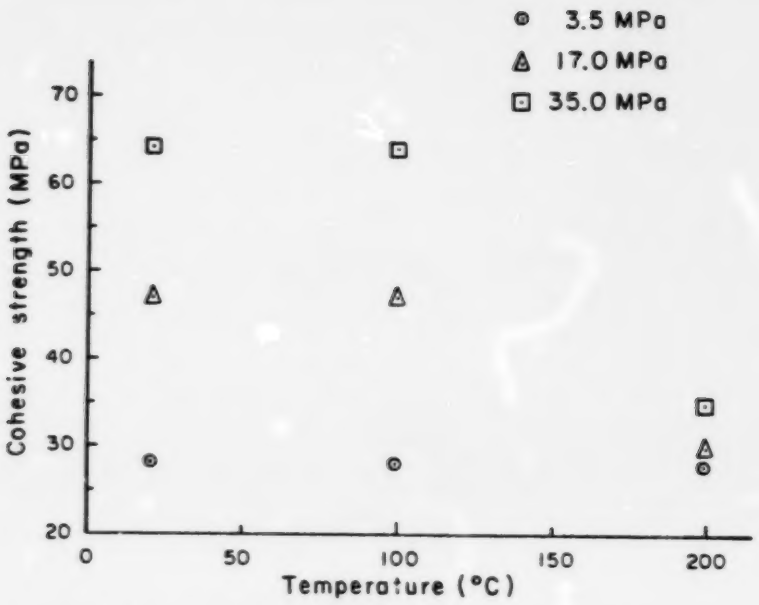

Fig. 18 - Cohesive strength vs temperature:
URL-6 224 - 260 m horizon

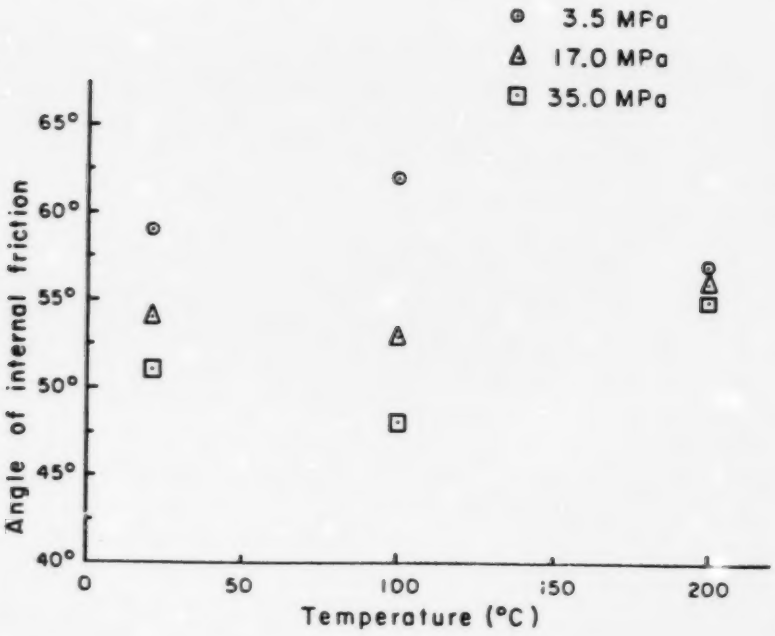

Fig. 19 - Angle of internal friction vs temperature:
URL-6 224 - 260 m horizon

APPENDIX A

FIG. A1: DEVIATORIAL STRESS VS STRAIN: URL6 224.50 (3.5 MPa)

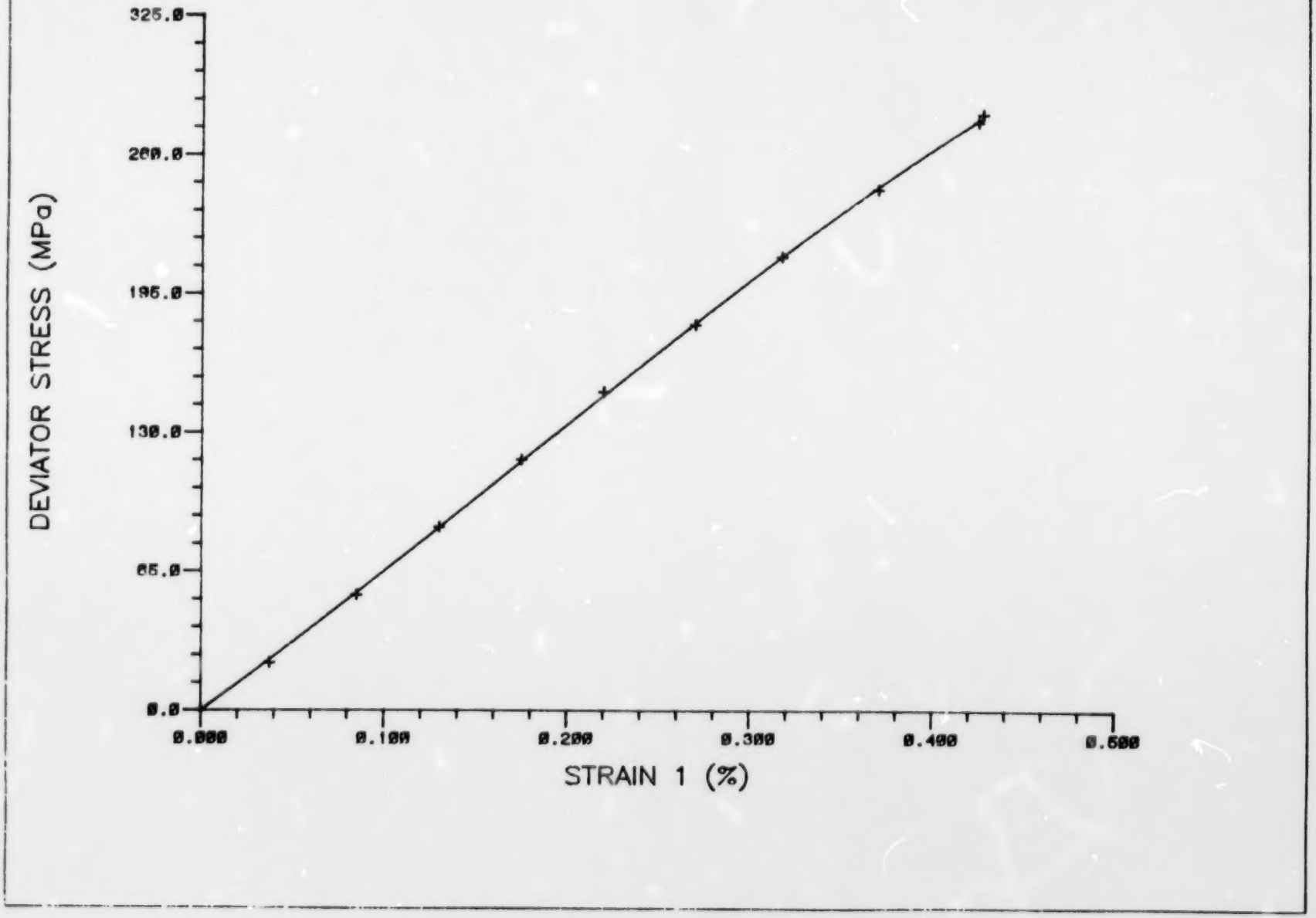

FIG. A2: DEVIATORIAL STRESS VS STRAIN: URL6 256.67 (3.5 MPa)

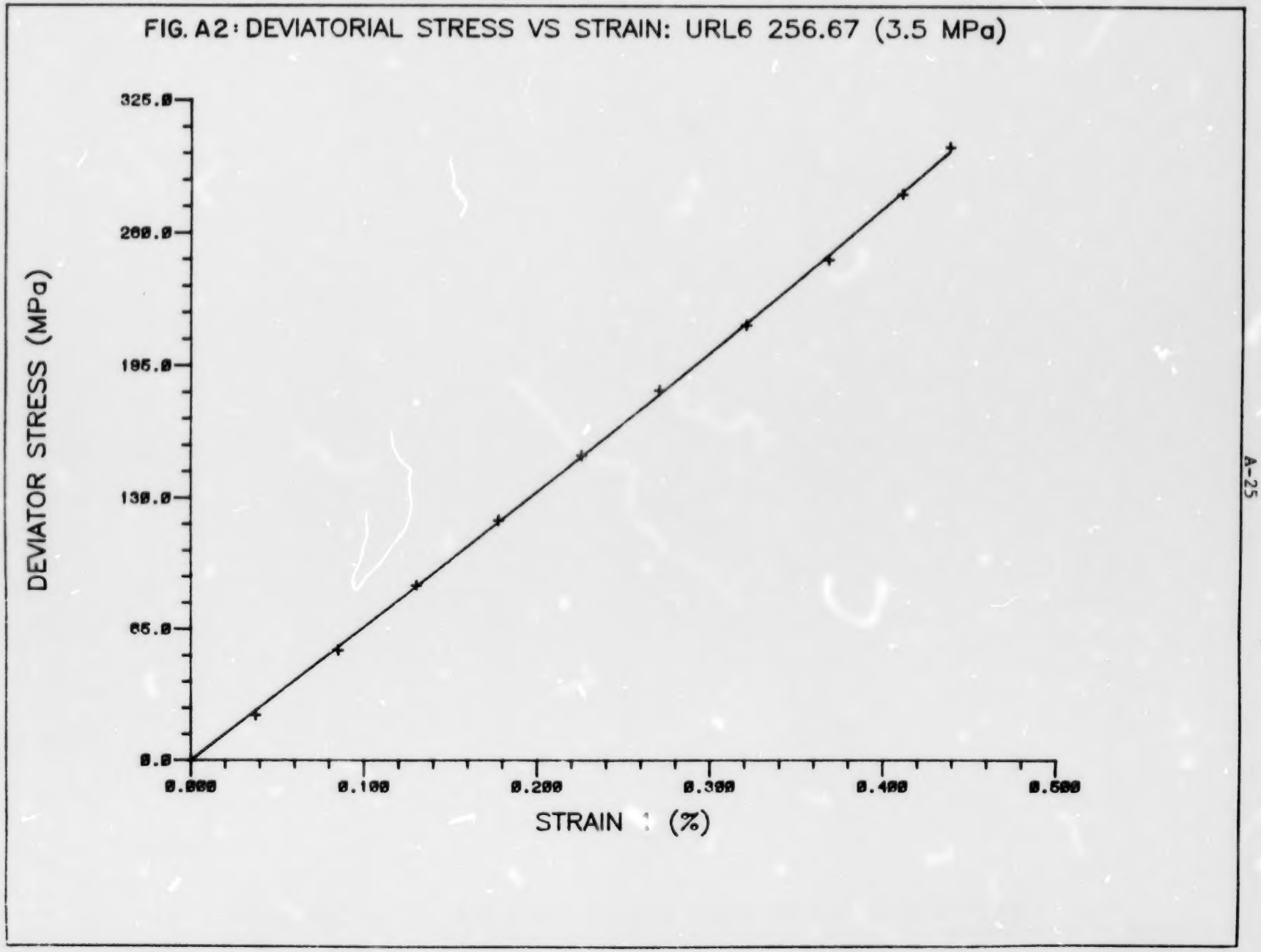

FIG. A3: DEVIATORIAL STRESS VS STRAIN: URL6 224.62 (10.0 MPa)

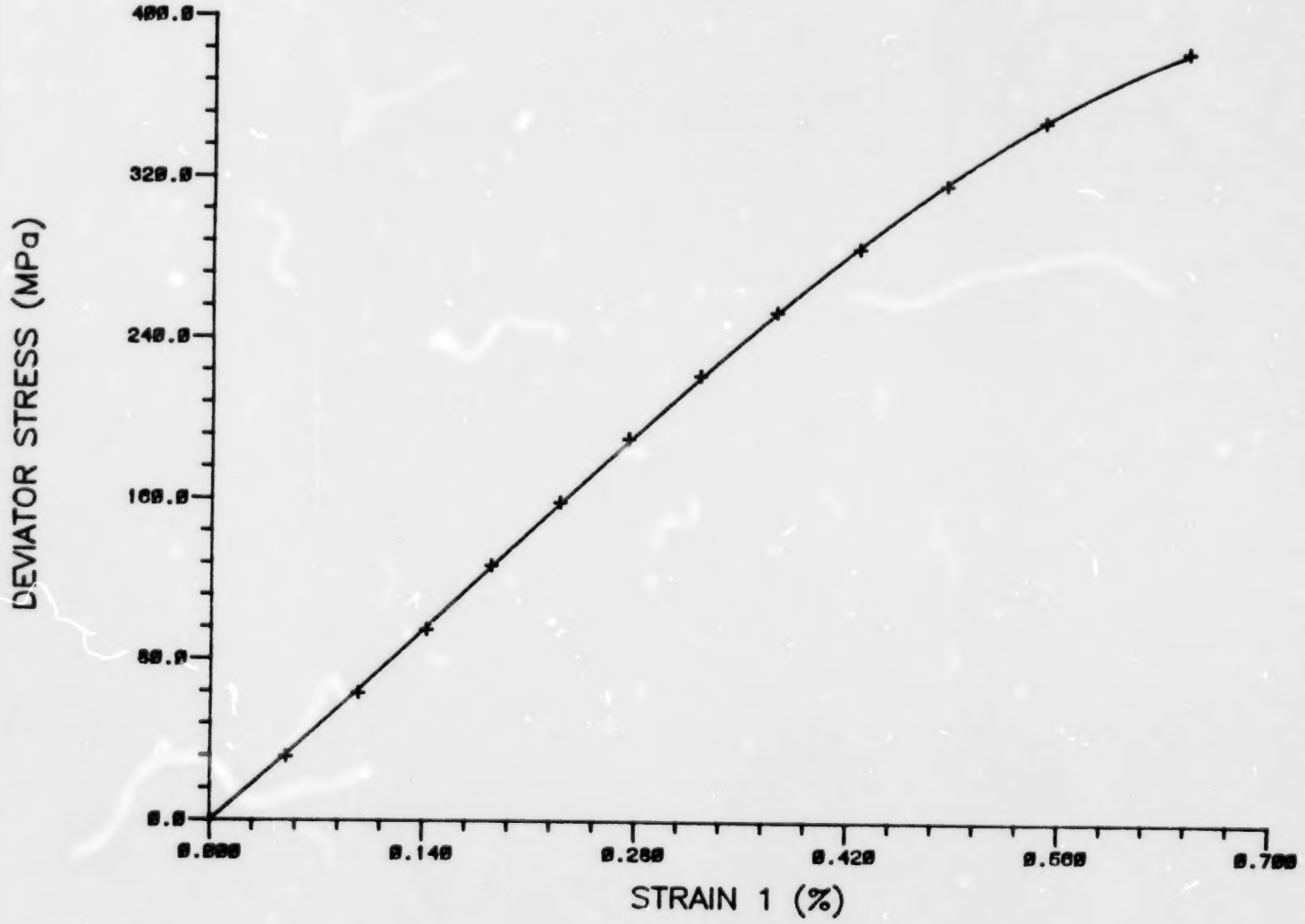

FIG. A4 : DEVIATORIAL STRESS VS STRAIN: URL6 257.60 (10.0 MPa)

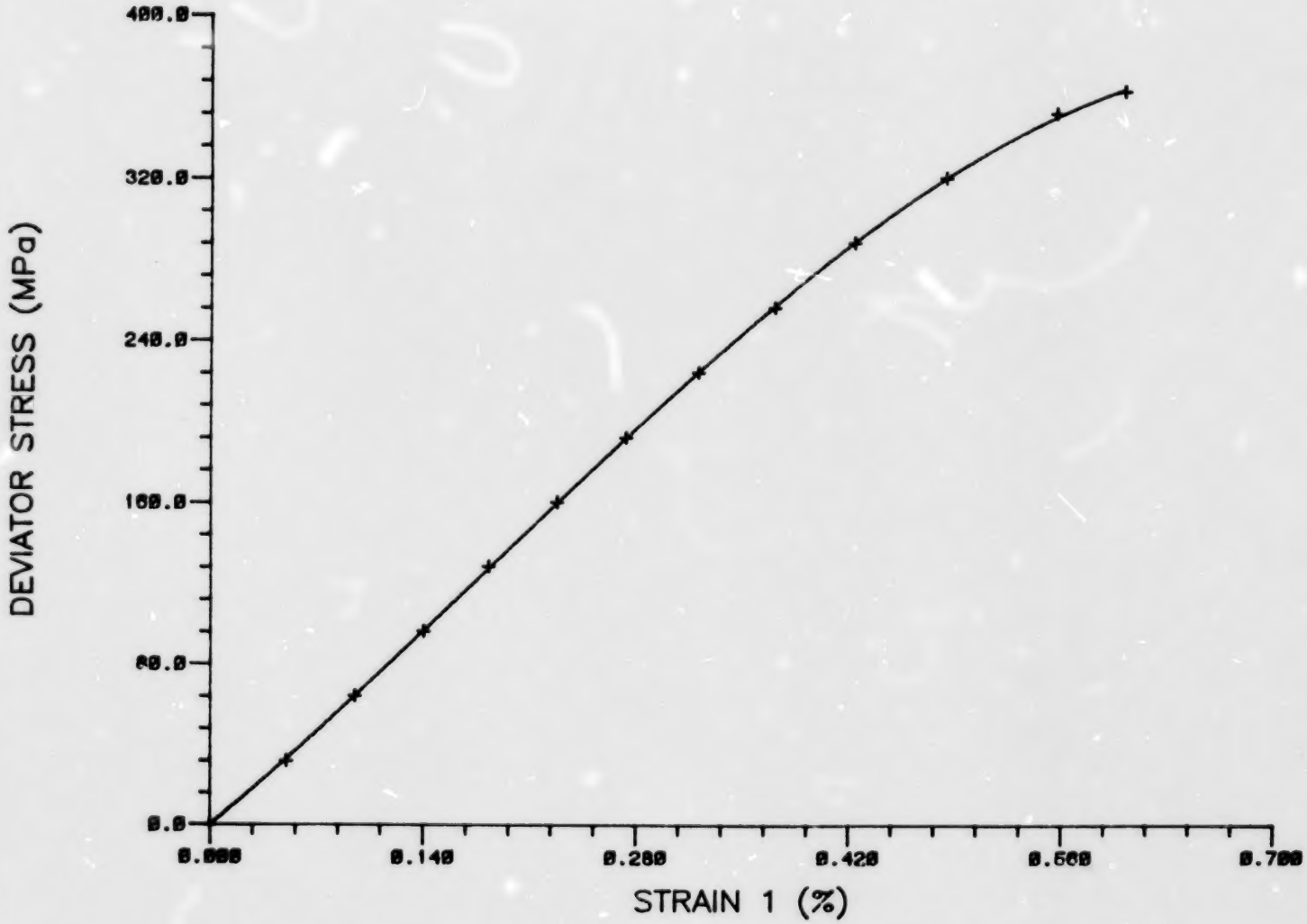

FIG. A5 : DEVIATORIAL STRESS VS STRAIN: URL6 224.74 (17.0 MPa)

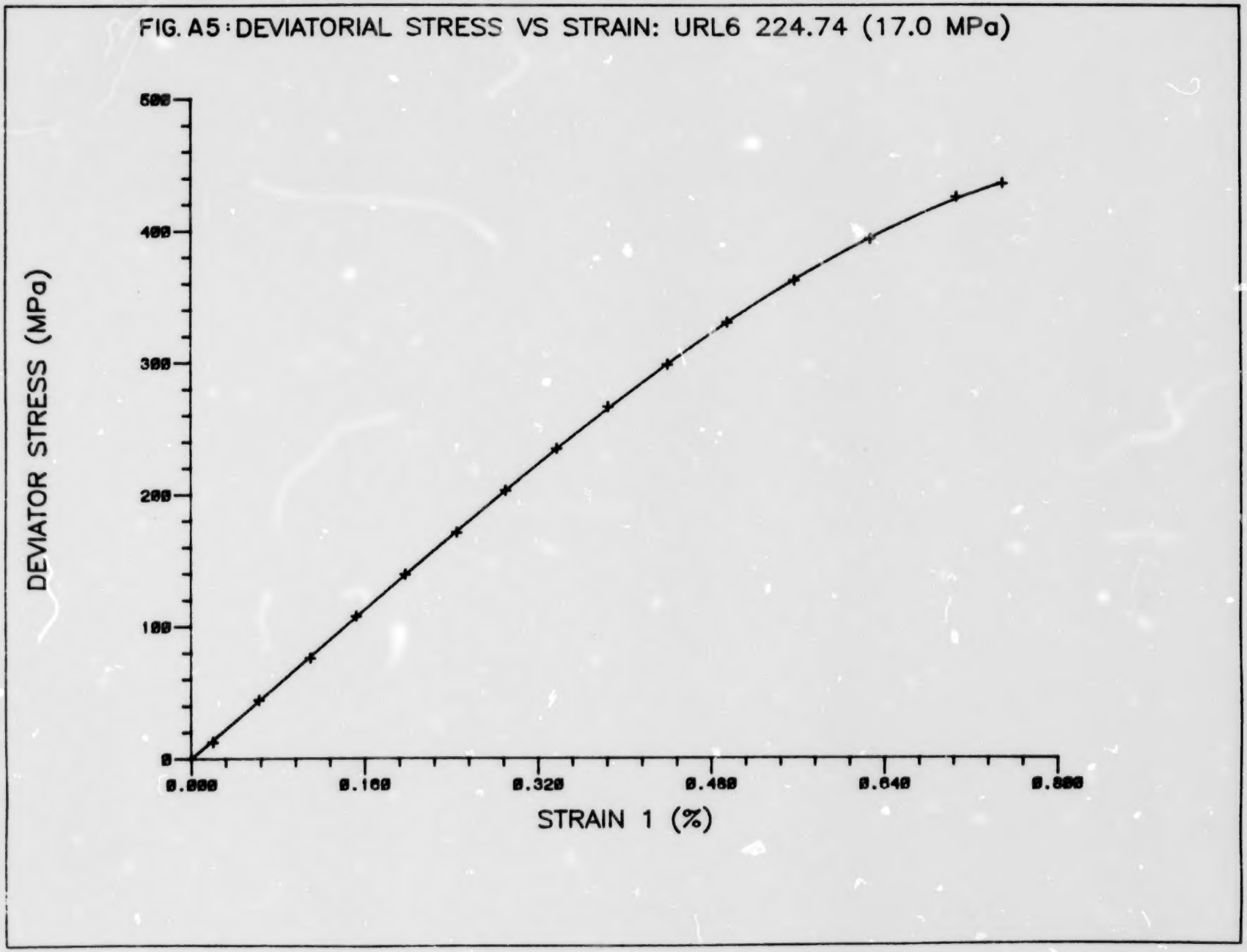

FIG. A6: DEVIATORIAL STRESS VS STRAIN: URL6 257.72 (17.0 MPa)

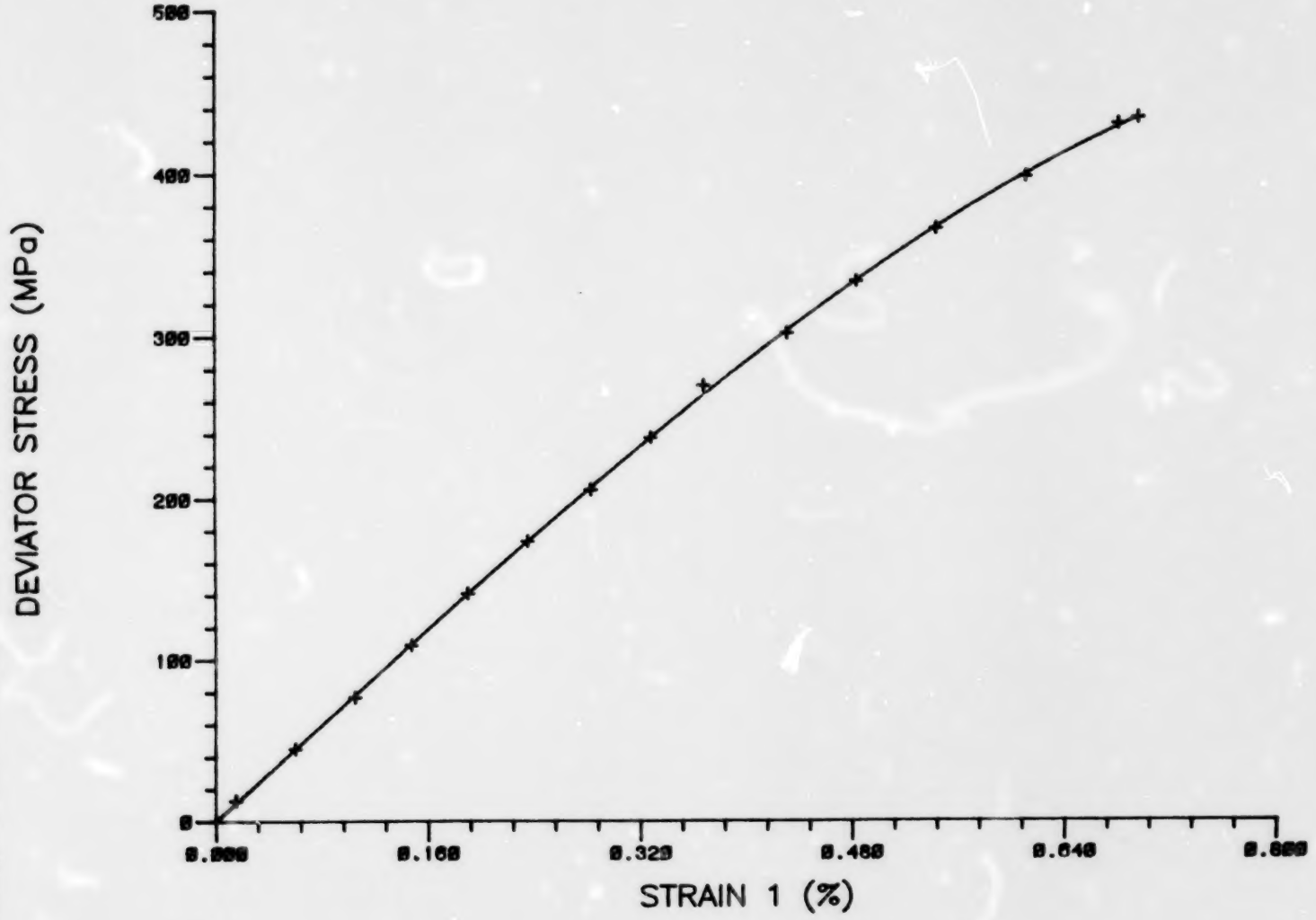

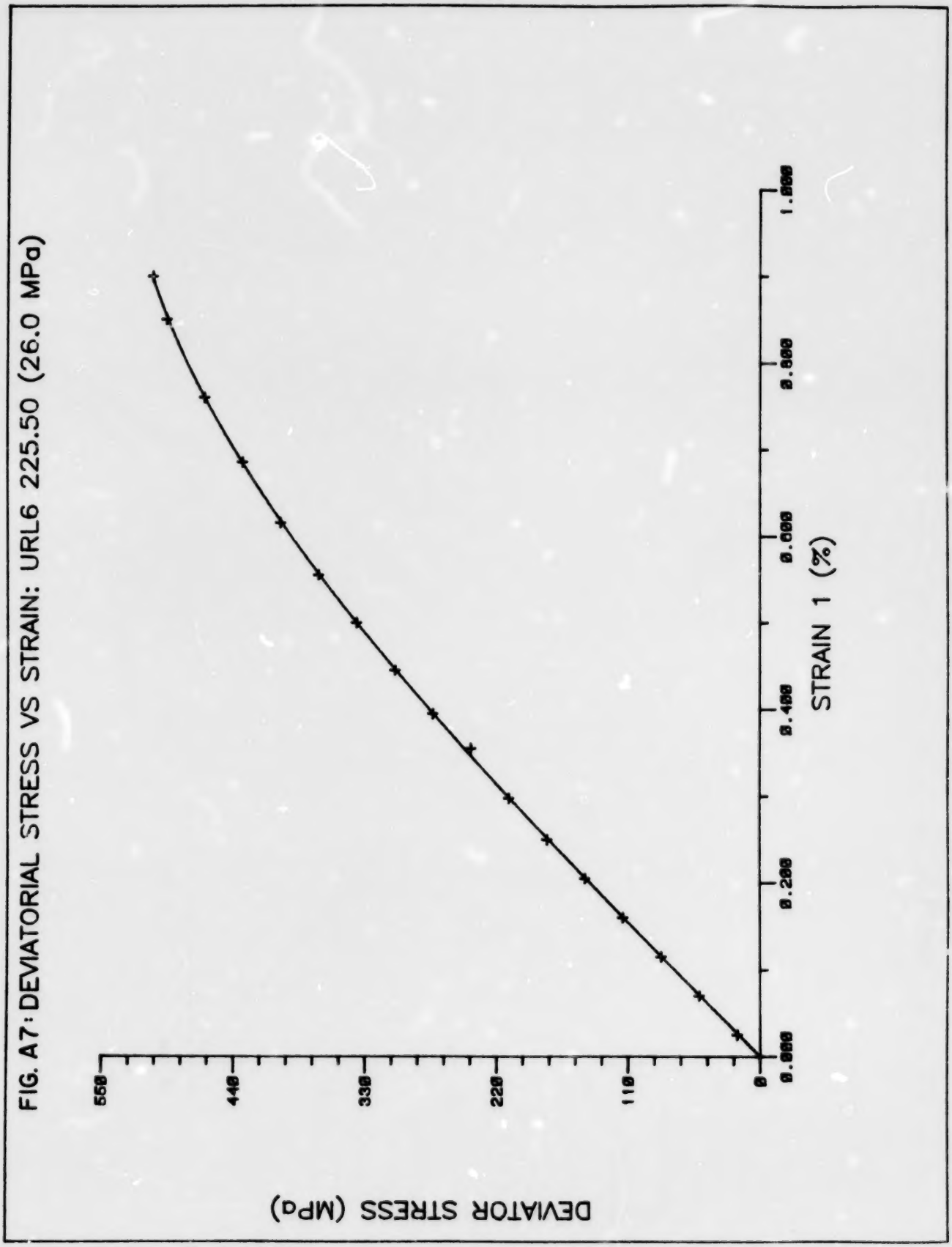

FIG. A7: DEVIATORIAL STRESS VS STRAIN: URL6 225.50 (26.0 MPa)

FIG. A8: DEVIATORIAL STRESS VS STRAIN: URL6 257.84 (26.0 MPa)

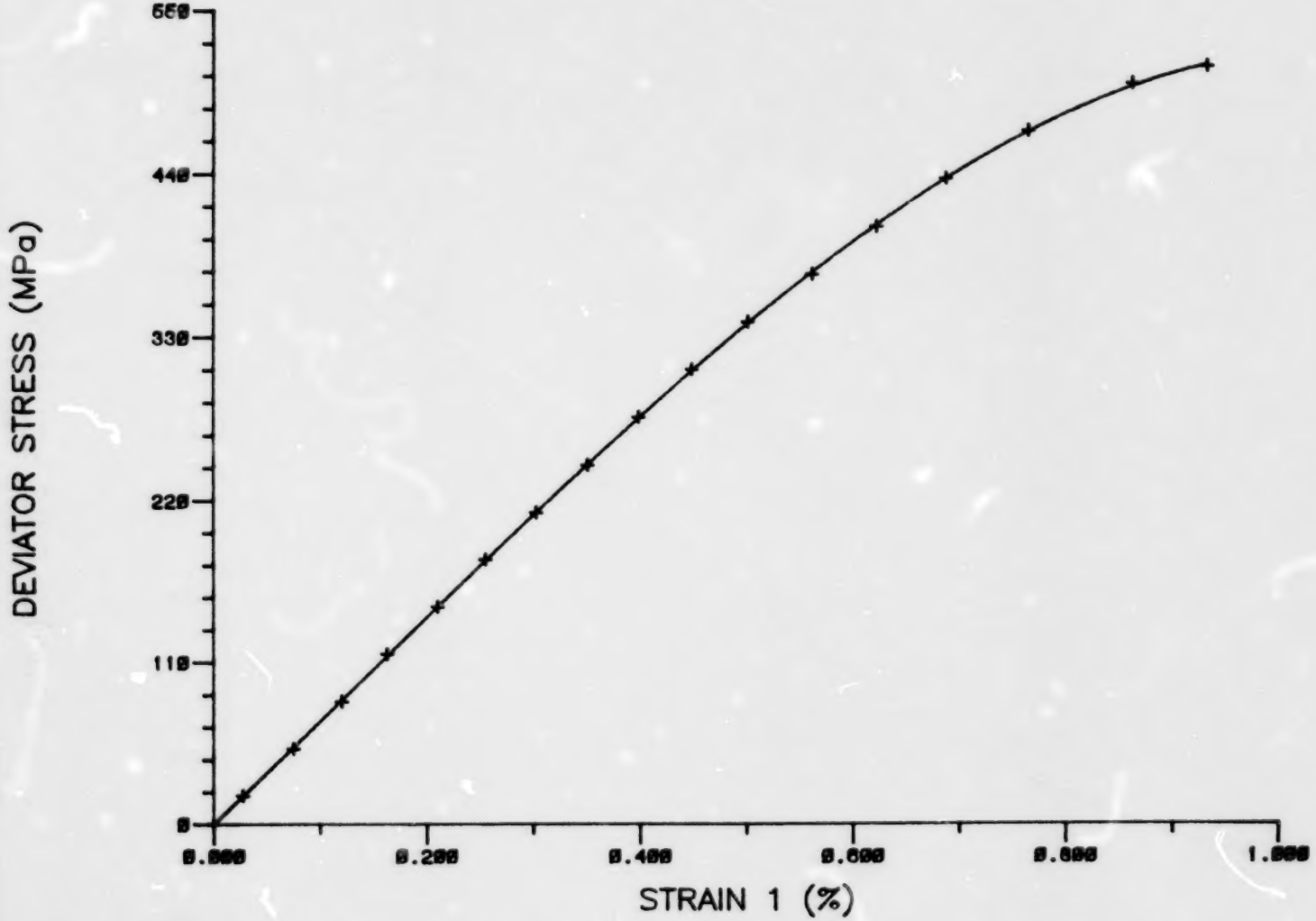

FIG. A9: DEVIATORIAL STRESS VS STRAIN: URL6 224.90 (35.0 MPa)

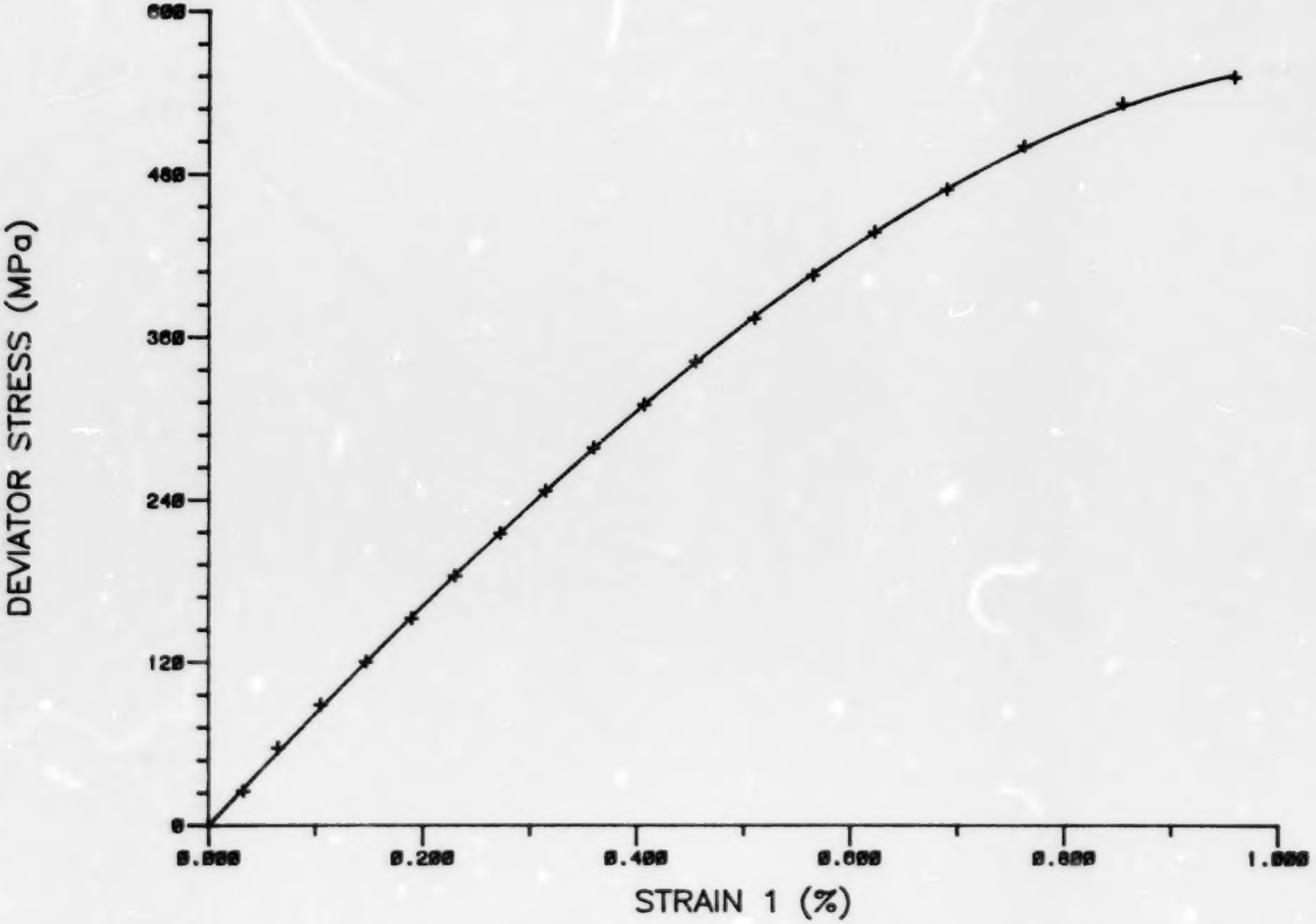

FIG. A10: DEVIATORIAL STRESS VS STRAIN: URL6 258.08 (35.0 MPa)

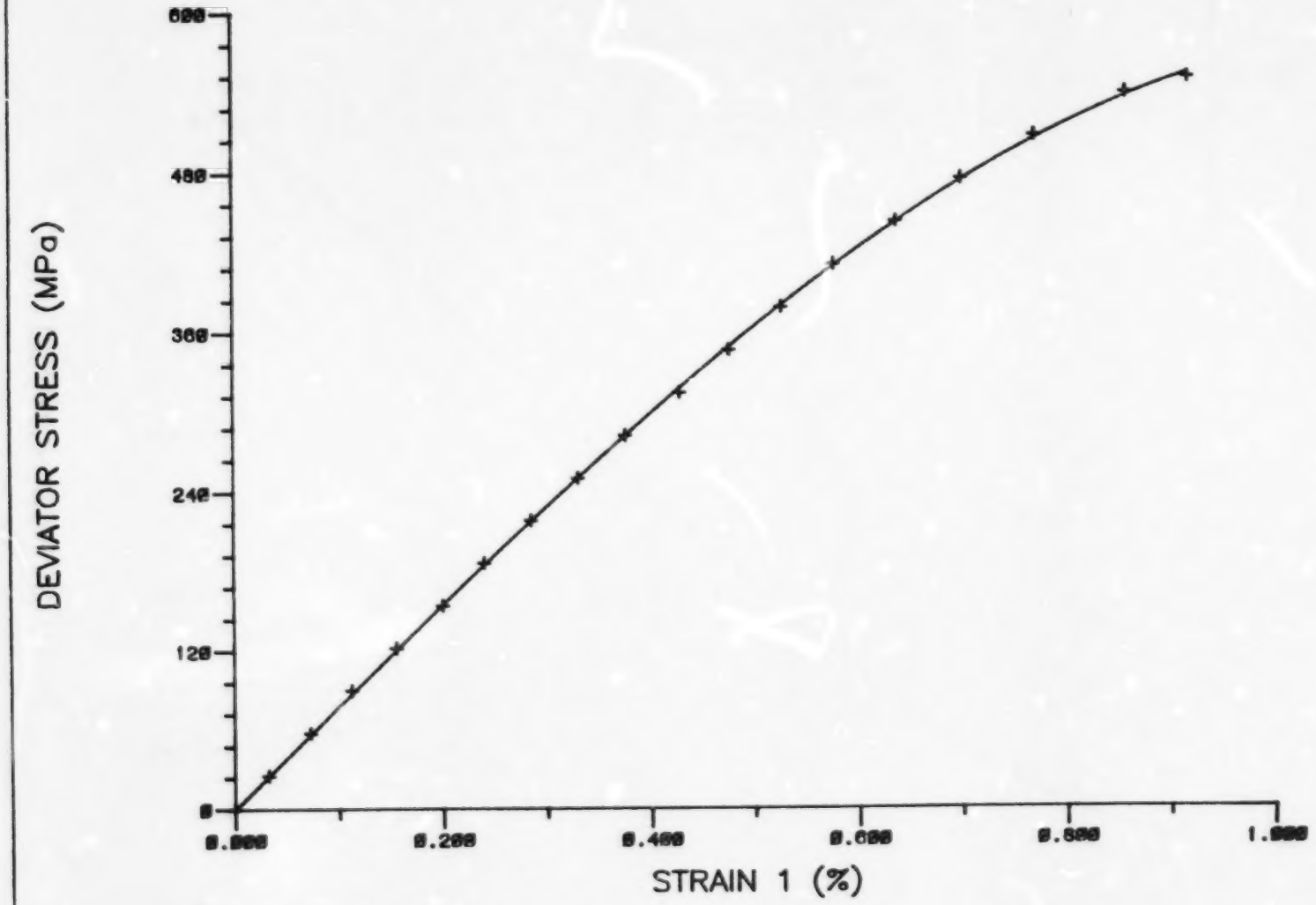

FIG. A11: DEVIATORIAL STRESS VS STRAIN: URL6 226.25 (3.5 MPa)

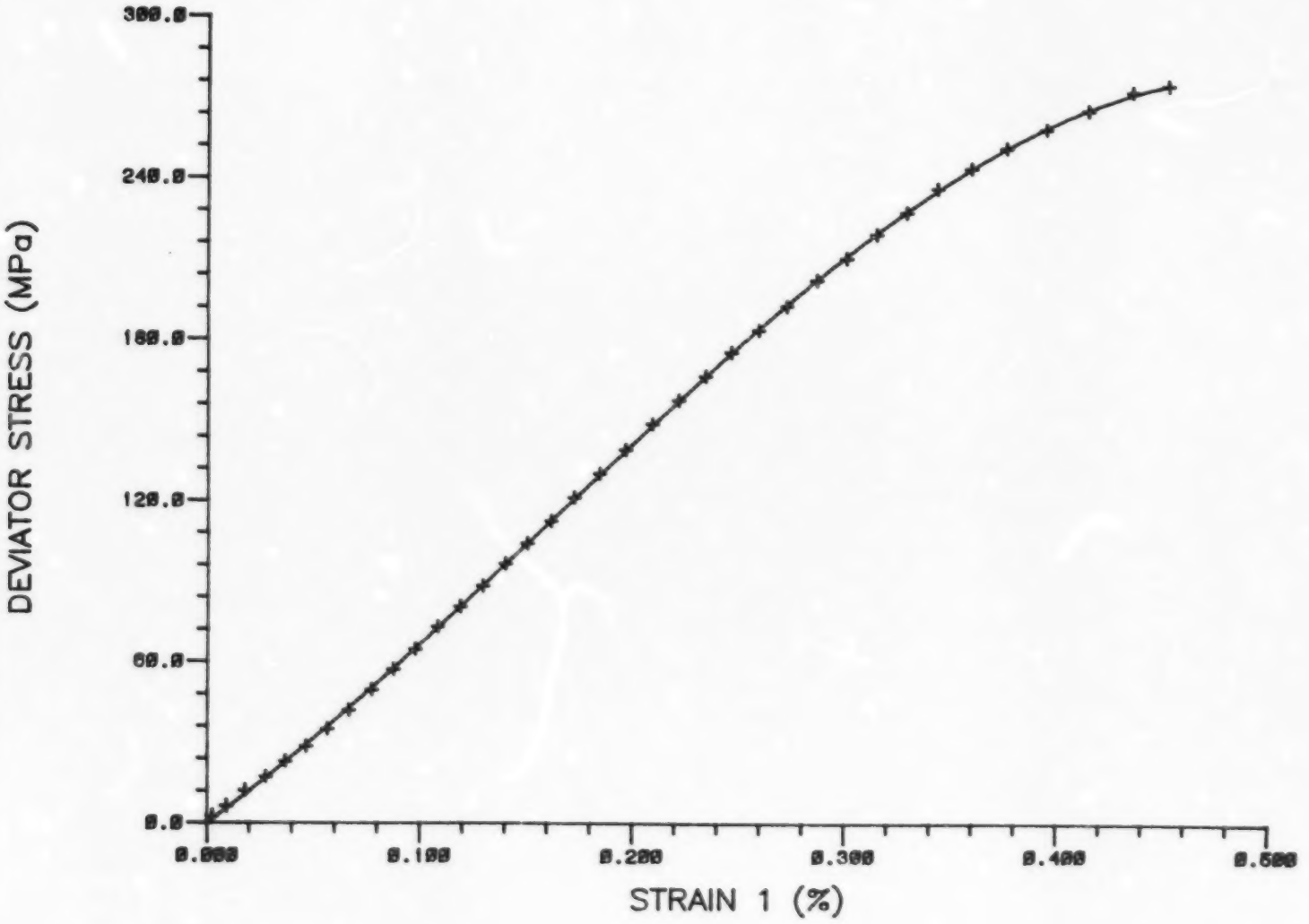

FIG. 12 : DEVIATORIAL STRESS VS STRAIN: URL6 256.51 (3.5 MPa)

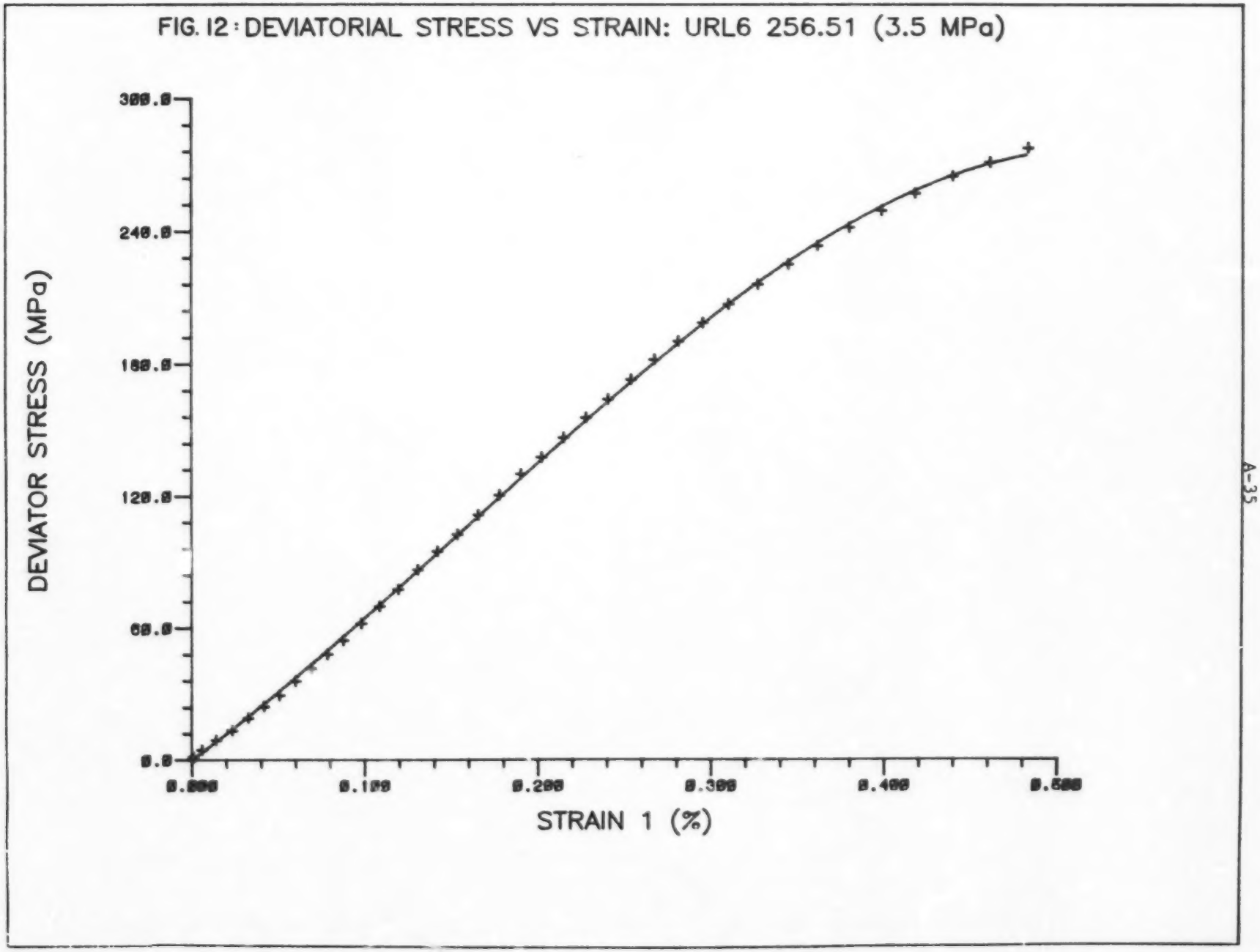

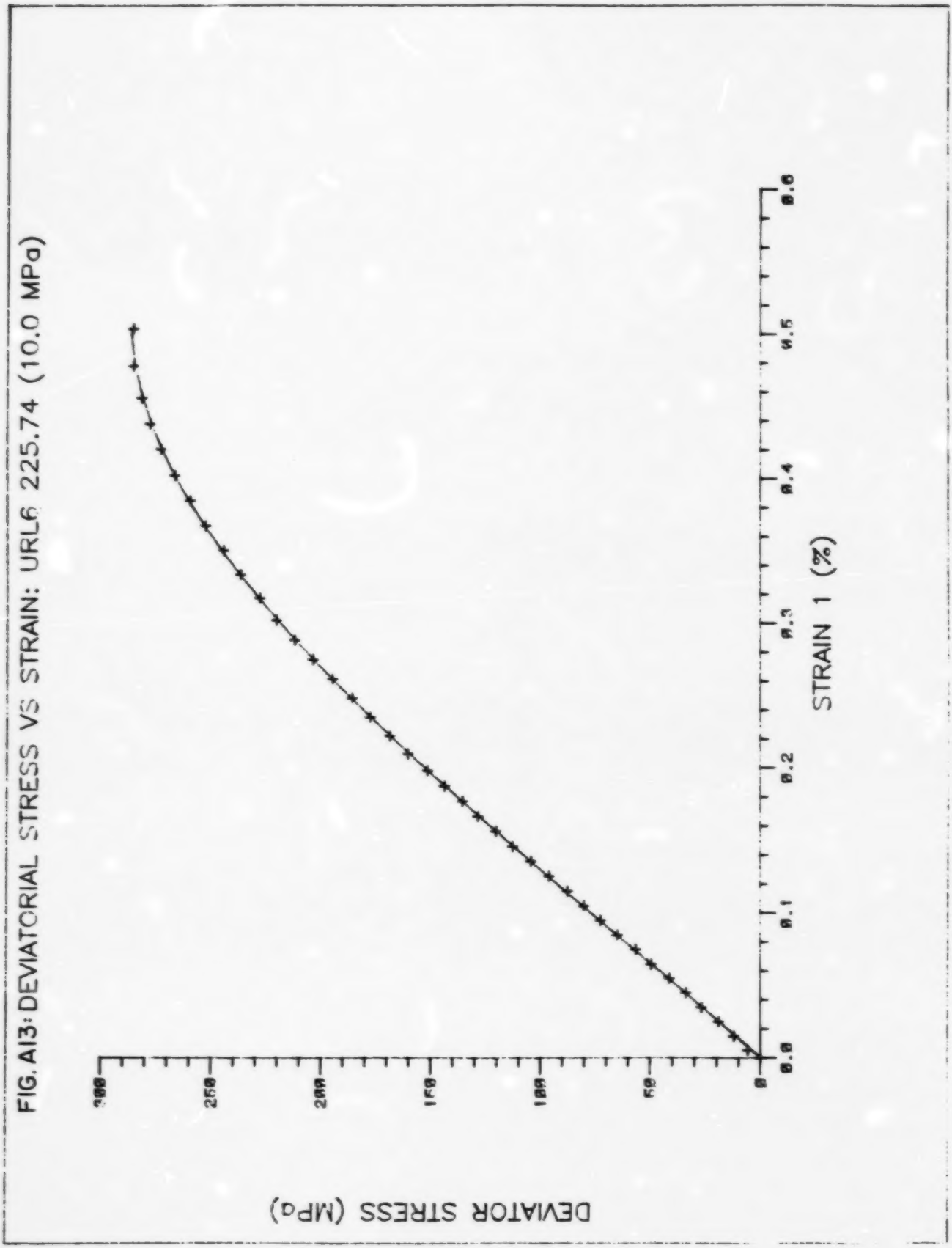
FIG. A13: DEVIATORIAL STRESS VS STRAIN: URL6 225.74 (10.0 MPa)
DEVIATOR STRESS (MPa)
STRAIN 1 (%)
0.0
0.1
0.2
0.3
0.4
0.5
0.6
0
50
100
150
200
250
300

FIG. A14: DEVIATORIAL STRESS VS STRAIN: URL6 258.20 (10.0 MPa)

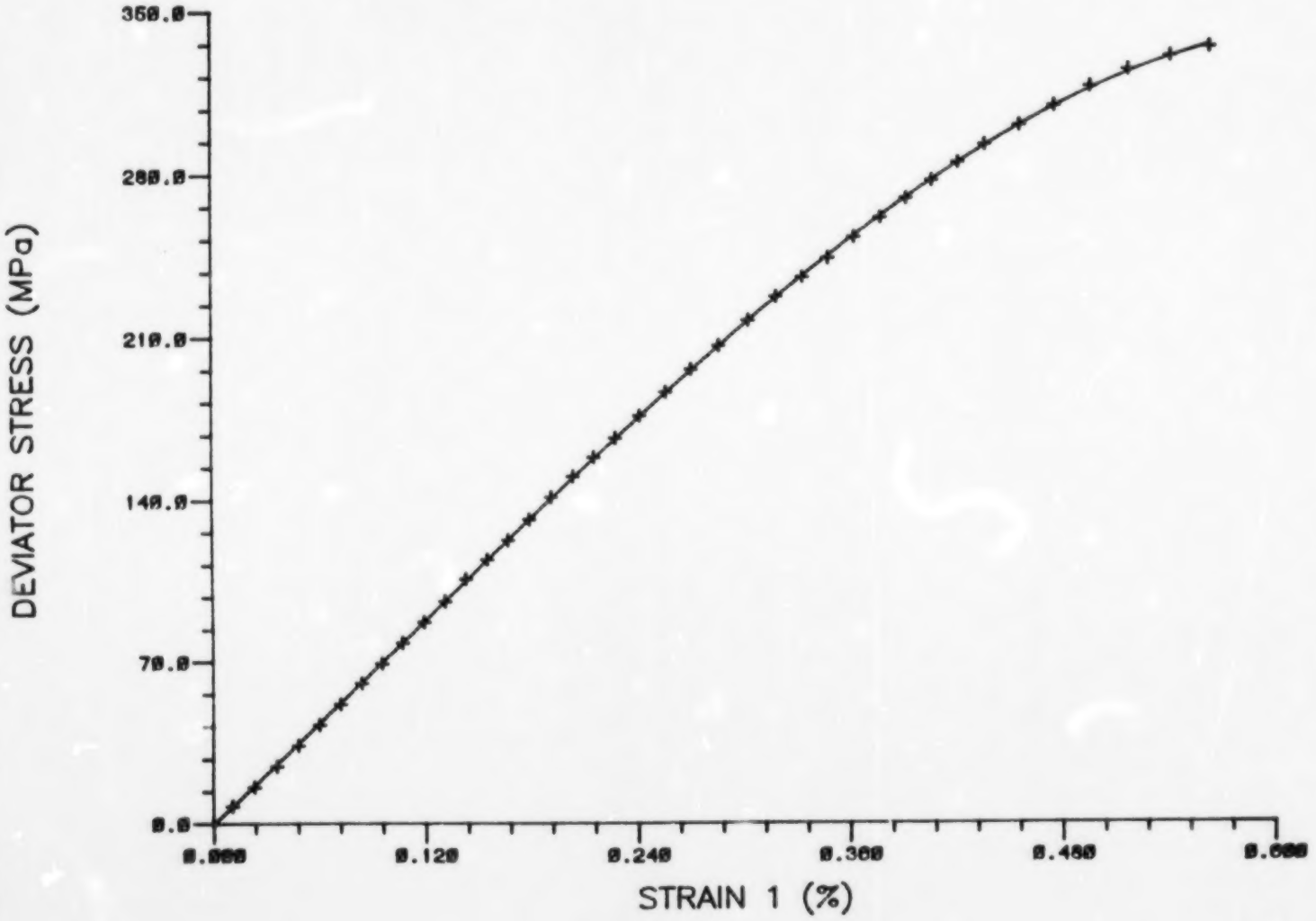

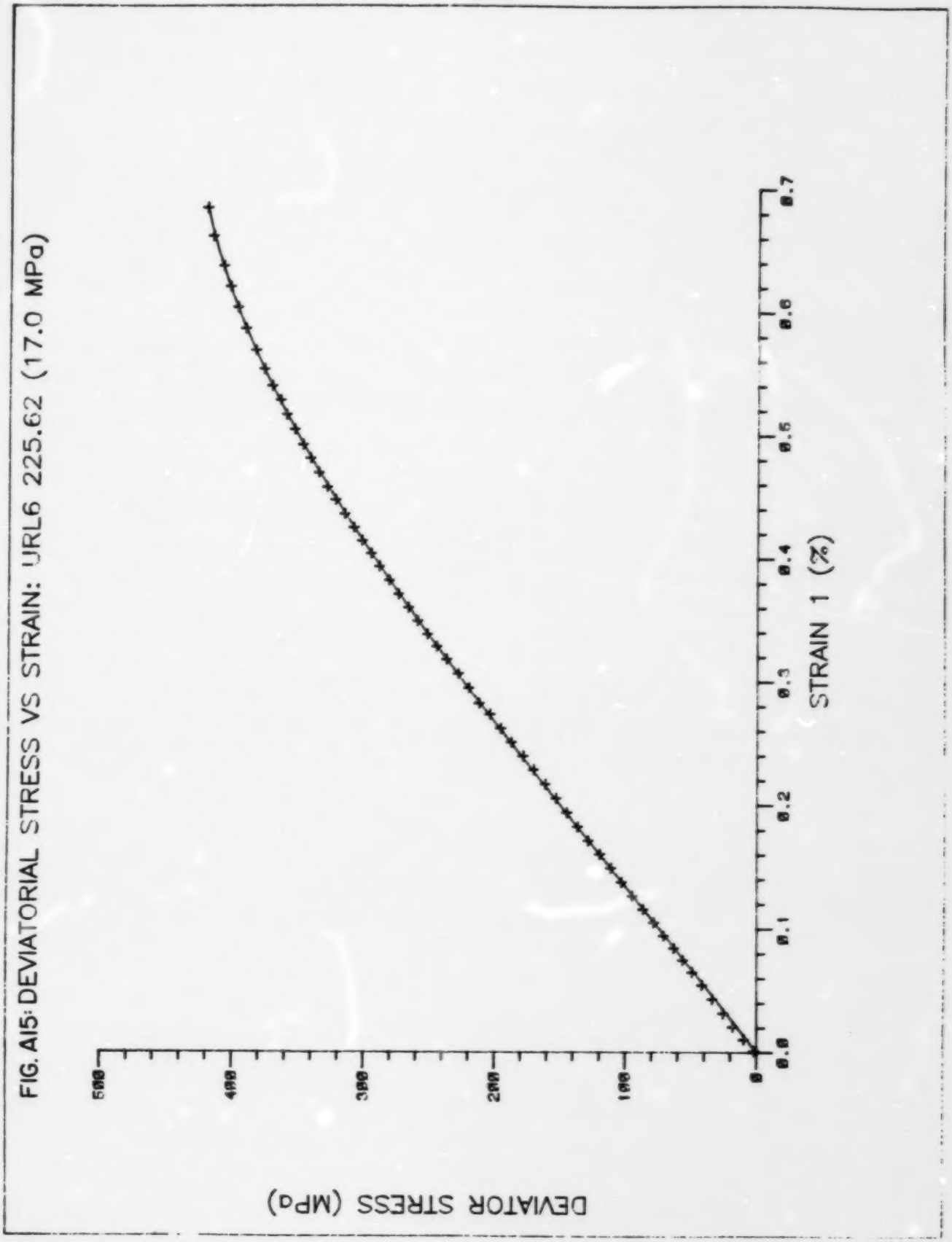
FIG. A15: DEVIATORIAL STRESS VS STRAIN: URL6 225.62 (17.0 MPa)
DEVIATOR STRESS (MPa)
500
400
300
200
100
0
0.0
0.1
0.2
0.3
0.4
0.5
0.6
0.7
STRAIN 1 (%)

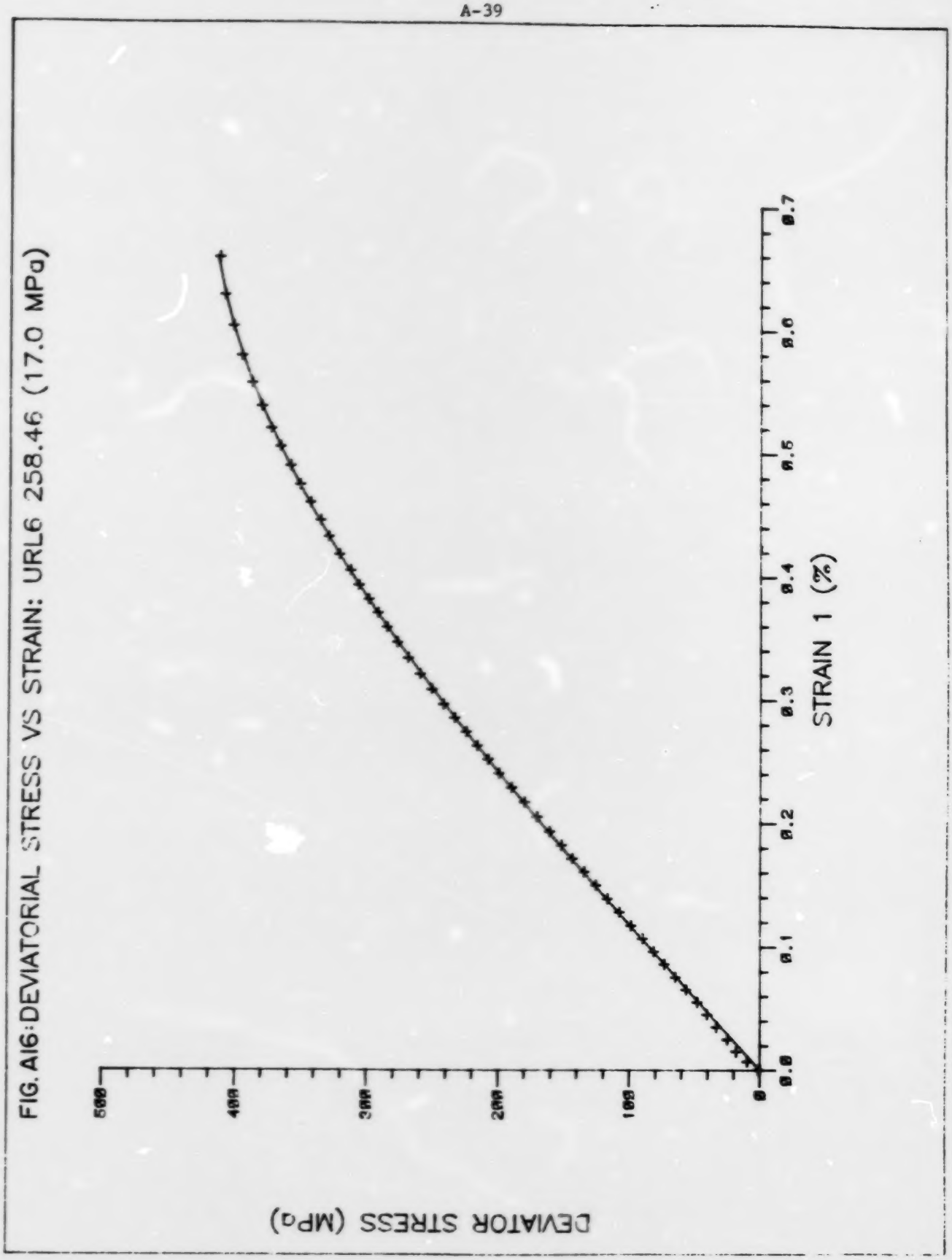
FIG. A16: DEVIATORIAL STRESS VS STRAIN: URL6 258.46 (17.0 MPa)
DEVIATOR STRESS (MPa)
500
400
300
200
100
0
0.0
0.1
0.2
0.3
0.4
0.5
0.6
0.7
STRAIN 1 (%)

FIG. A17: DEVIATORIAL STRESS VS STRAIN: URL6 225.90 (26.0 MPa)

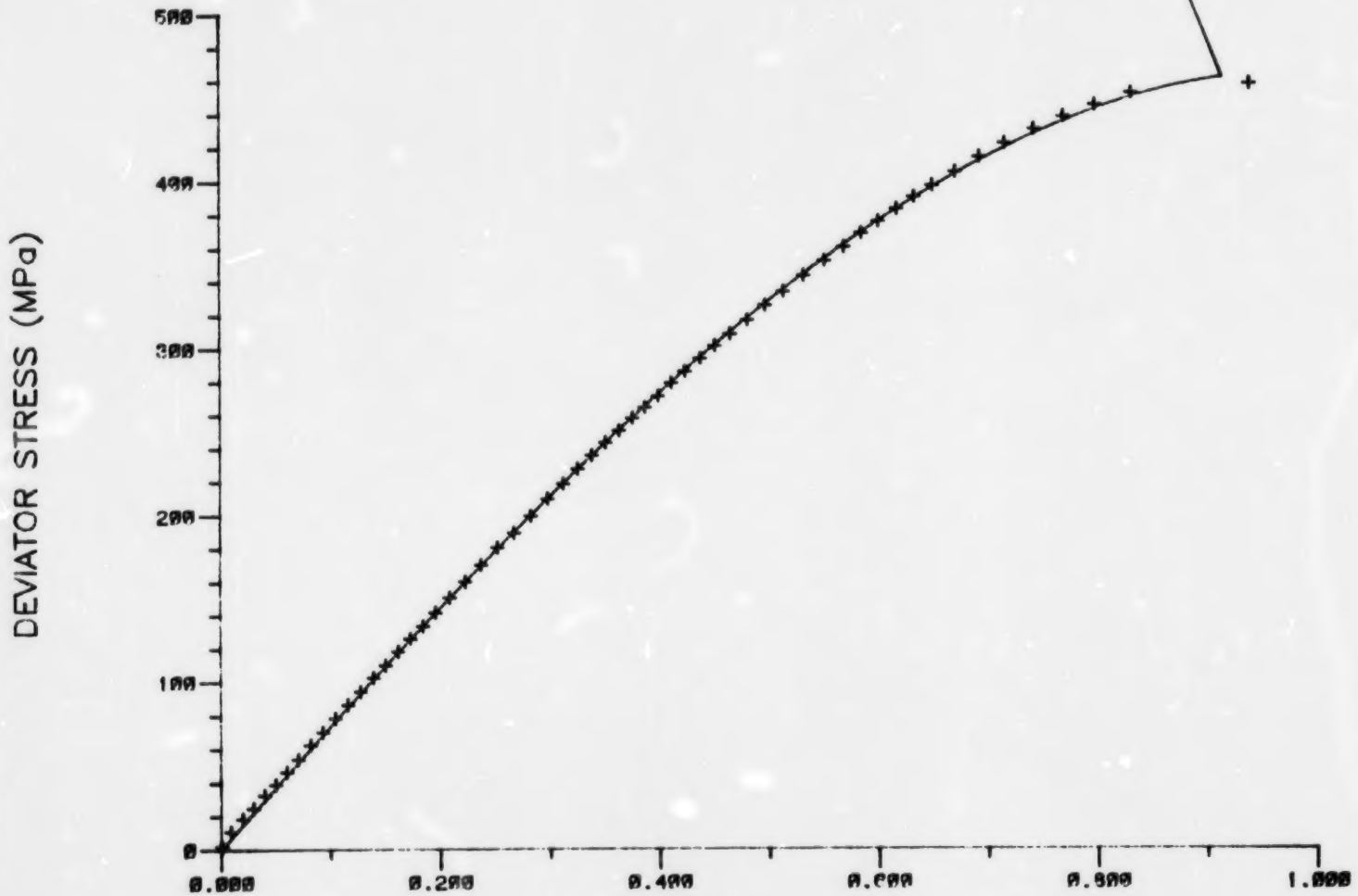

FIG. A18: DEVIATORIAL STRESS VS STRAIN: URL6 258.82 (26.0 MPa)

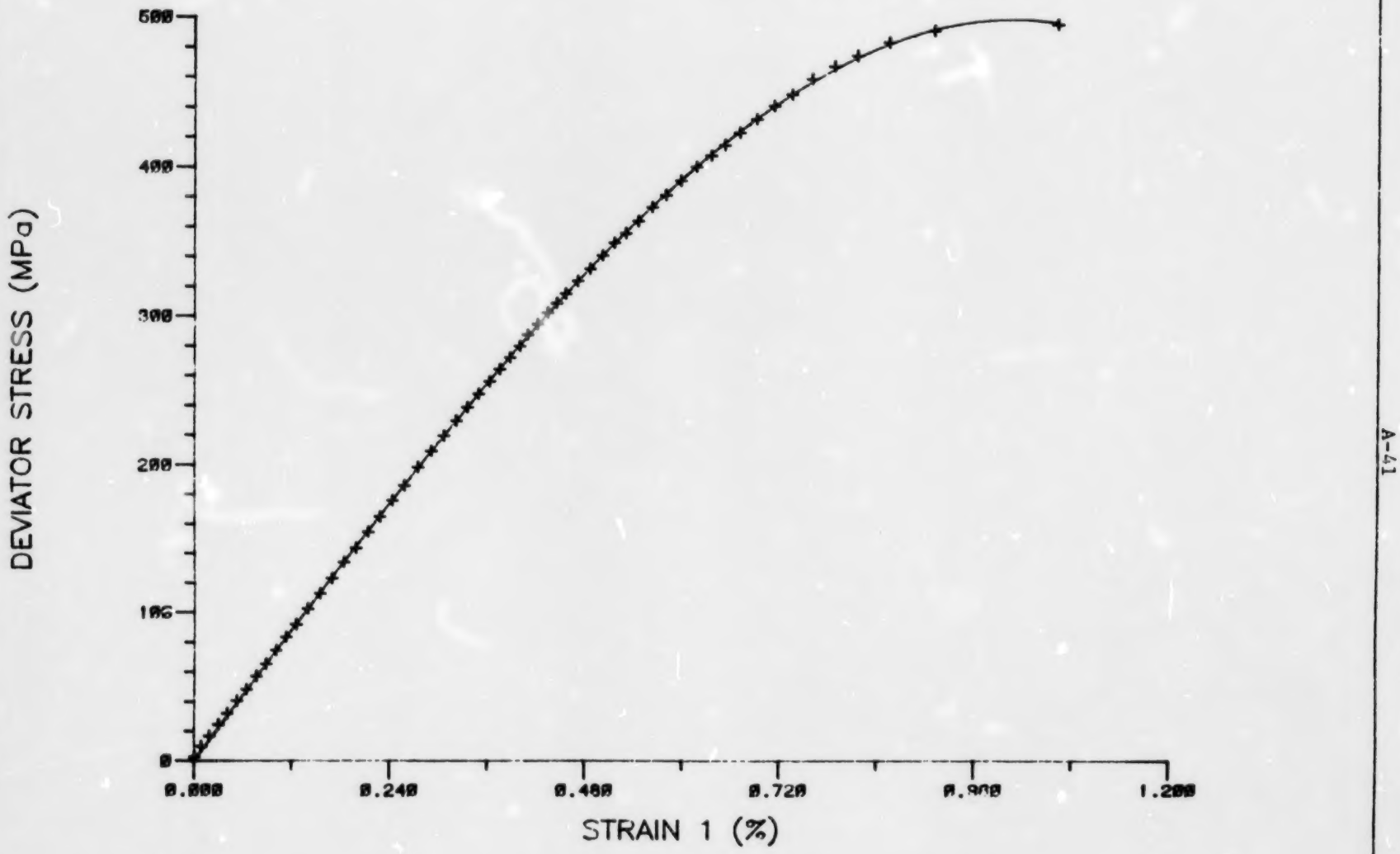

FIG. A19: DEVIATORIAL STRESS VS STRAIN: URL6 226.02 (35.0 MPa)

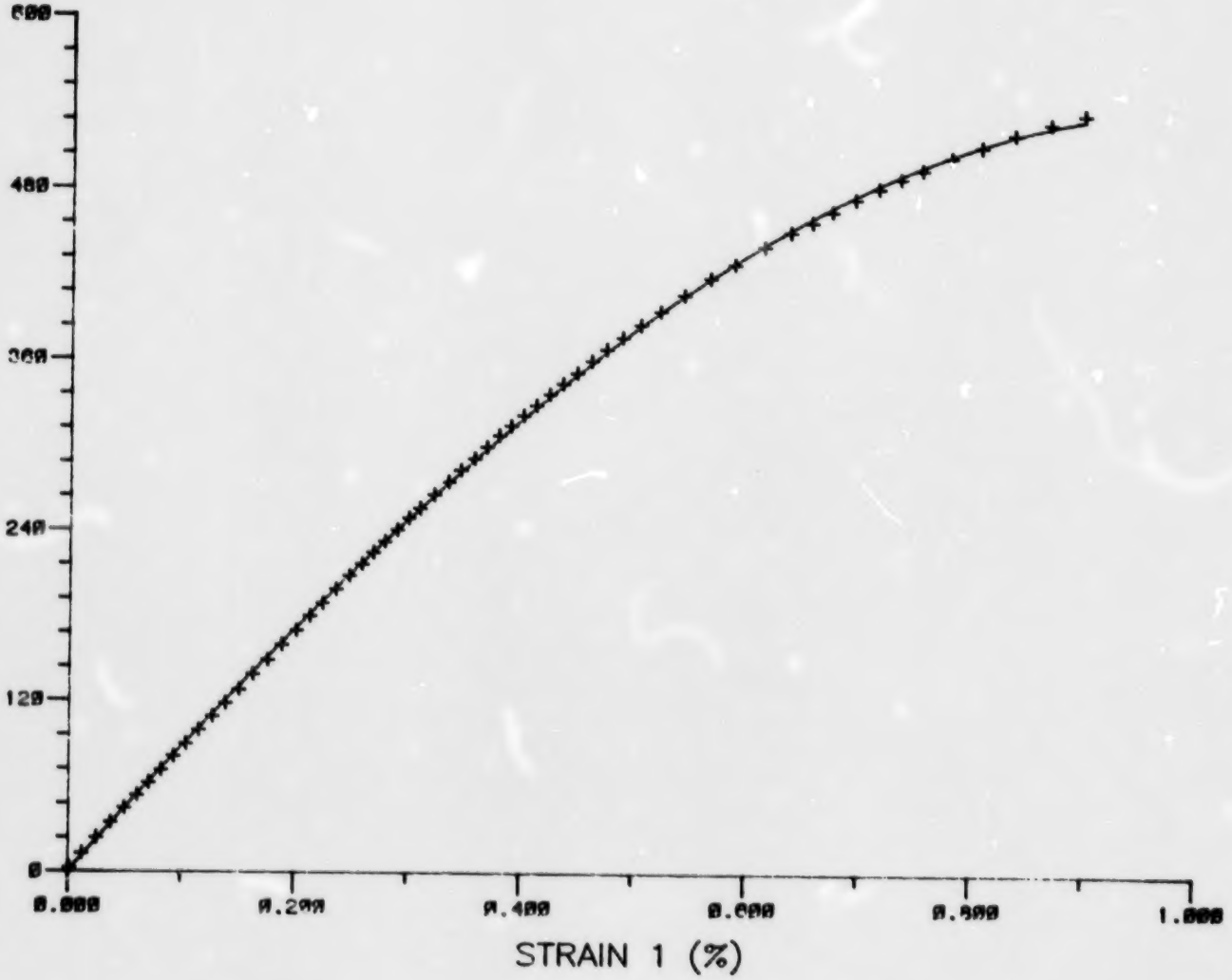

FIG. A20: DEVIATORIAL STRESS VS STRAIN: URL6 258.70 (35.0 MPa)

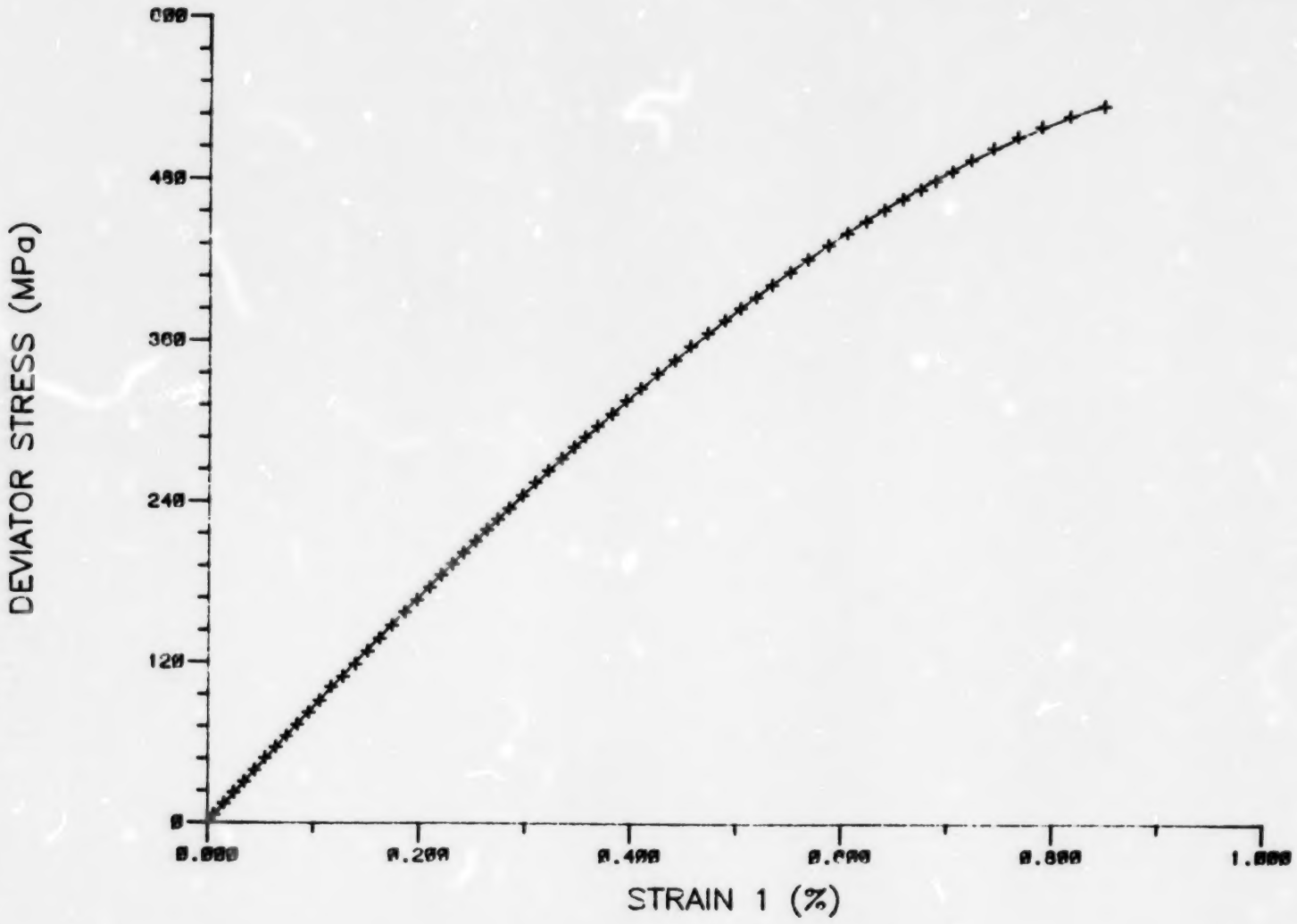

FIG. A21: DEVIATORIAL STRESS VS STRAIN: URL6 226.37 (3.5 MPa)

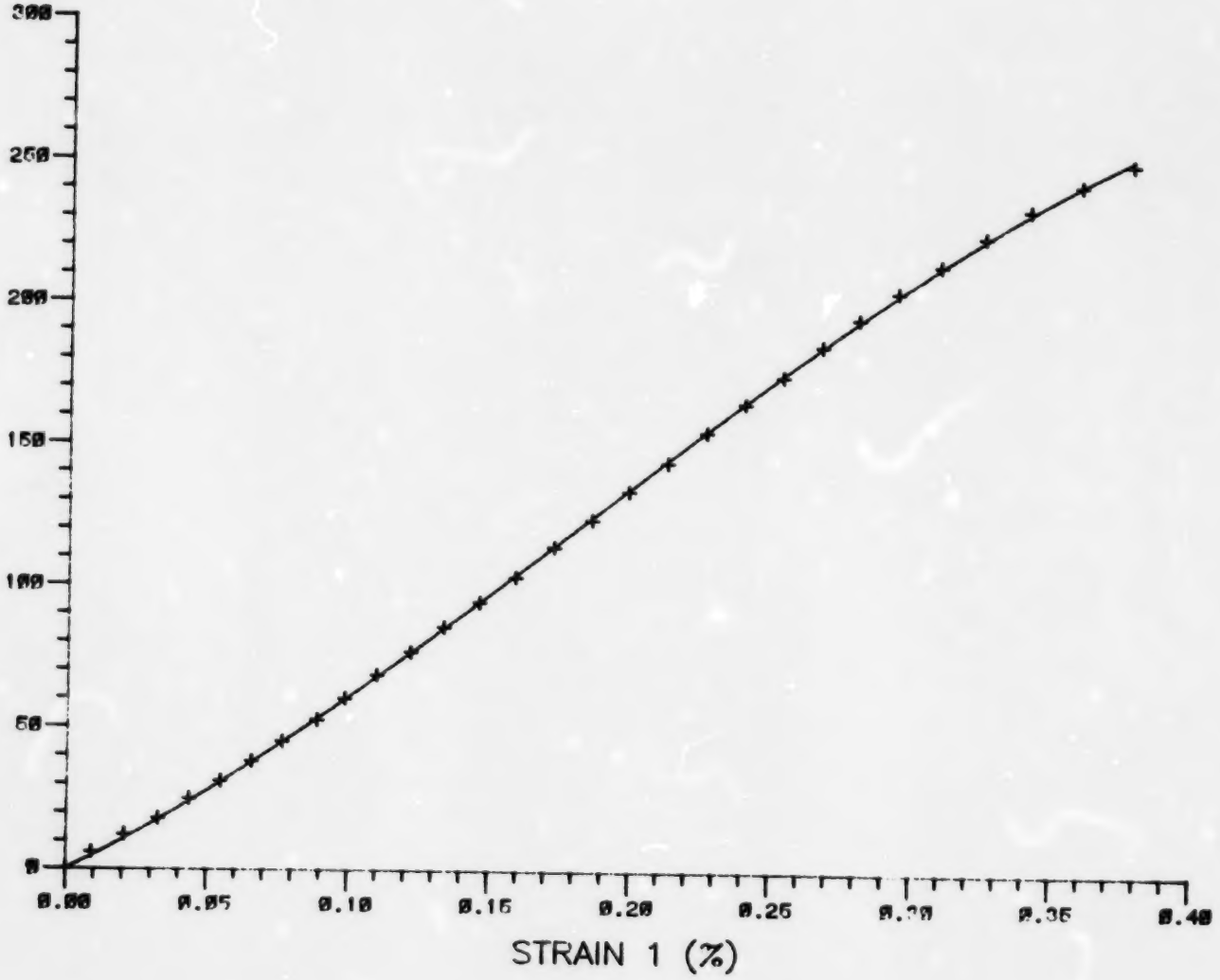

FIG. A22: DEVIATORIAL STRESS VS STRAIN: URL6 227.42 (3.5 MPa)

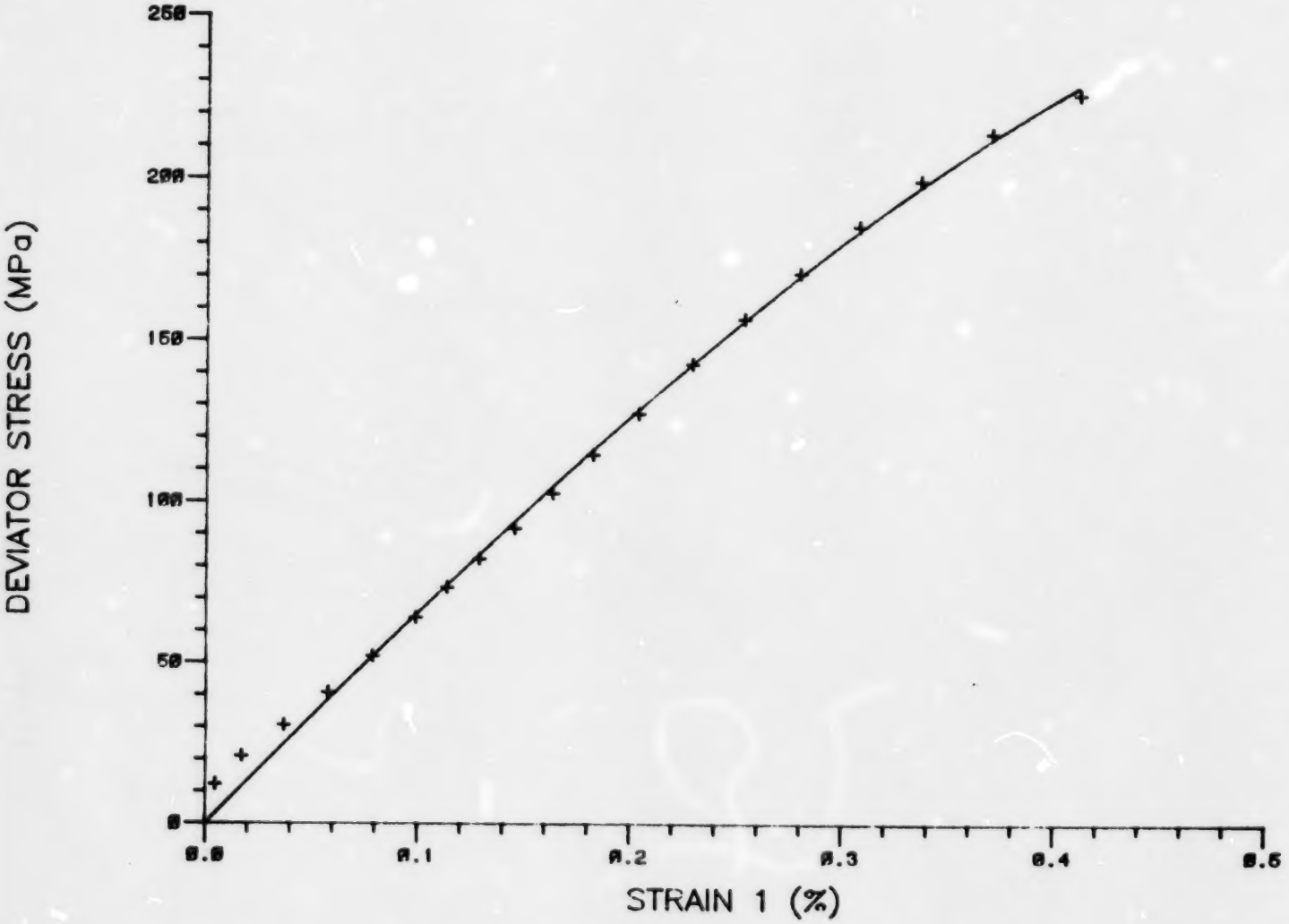

FIG. A23: DEVIATORIAL STRESS VS STRAIN: URL6 228.45 (3.5 MPa)

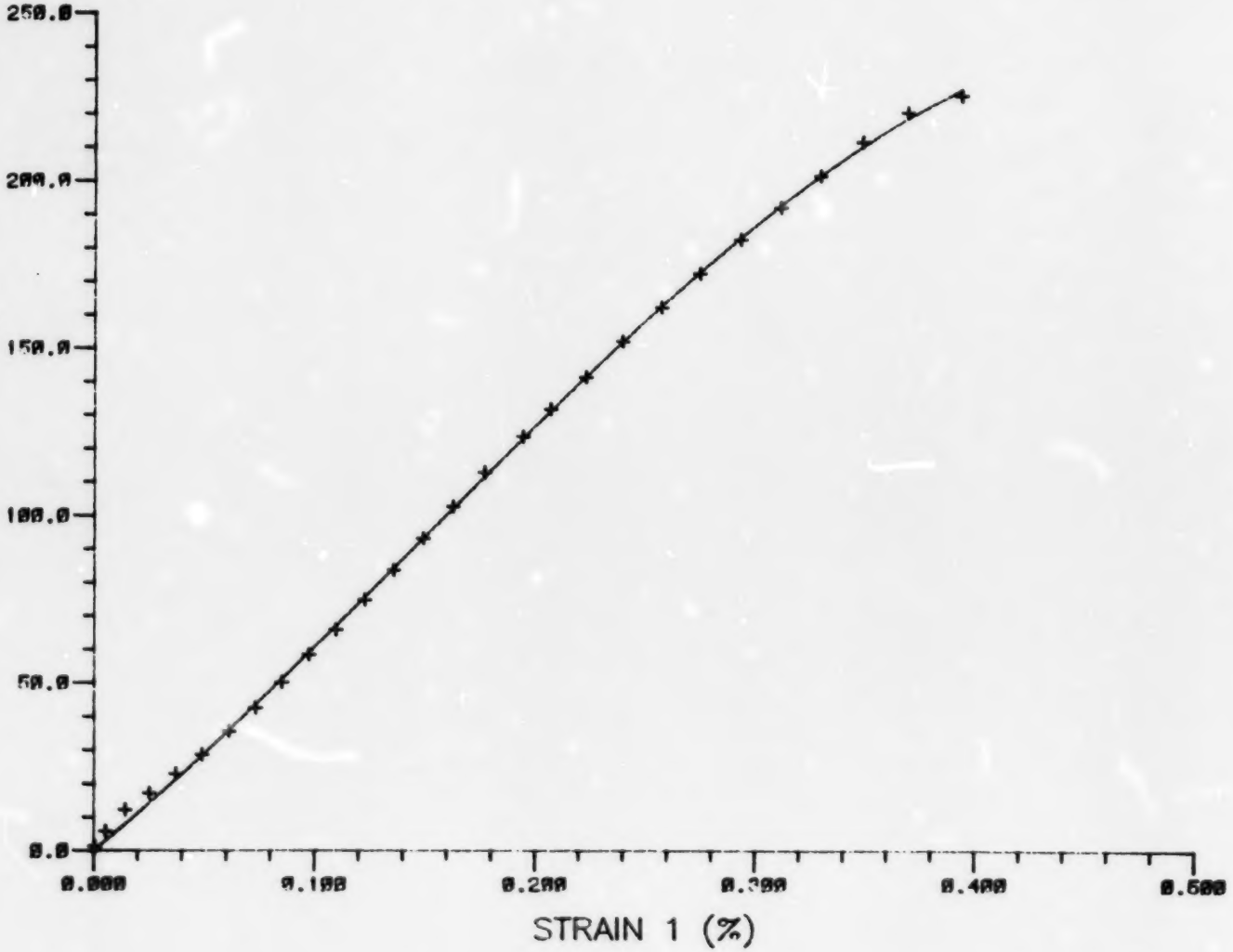

FIG. A24: DEVIATORIAL STRESS VS STRAIN: URL6 226.60 (10.0 MPa)

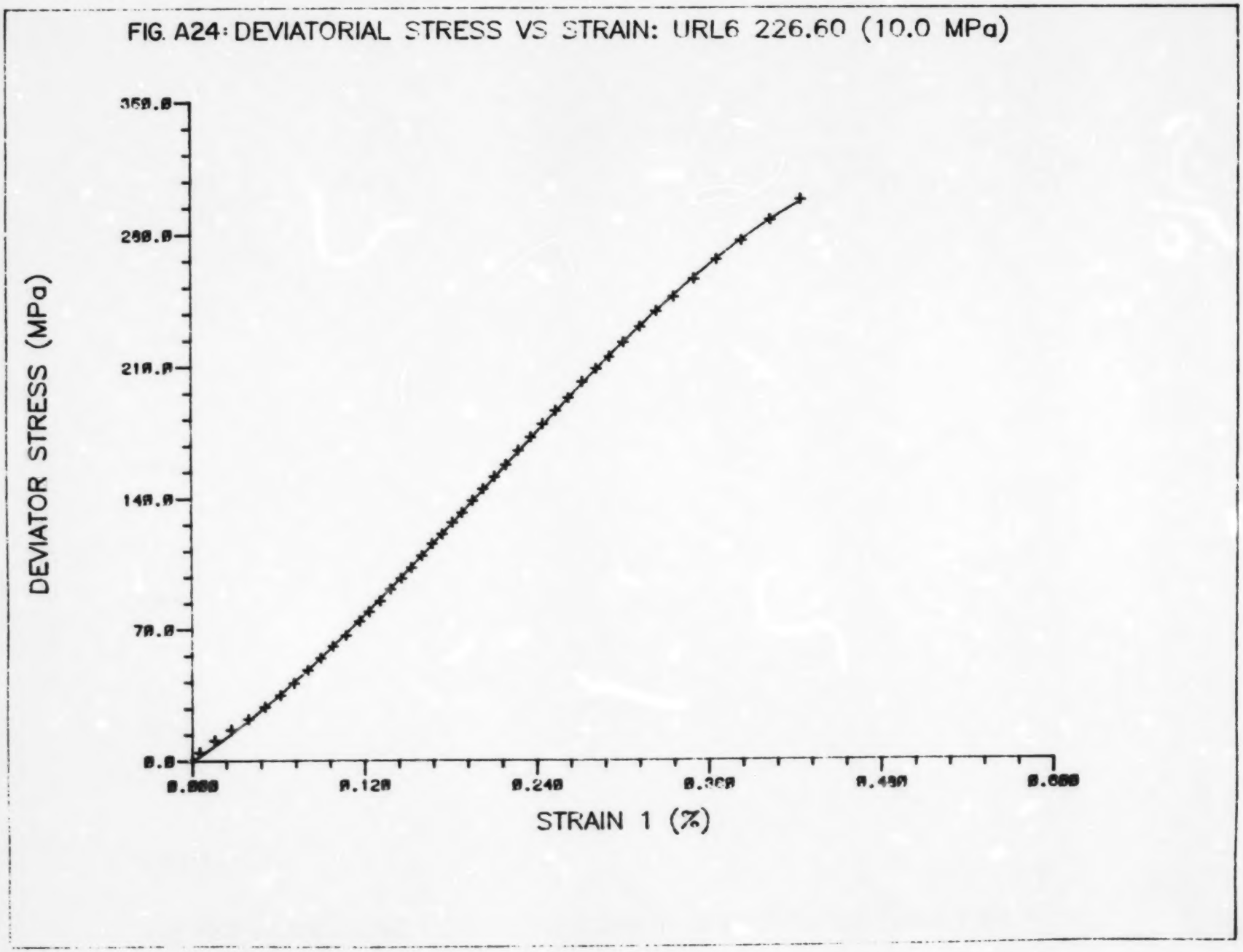

FIG. A25: DEVIATORIAL STRESS VS STRAIN: URL6 228.33 (10.0 MPa)

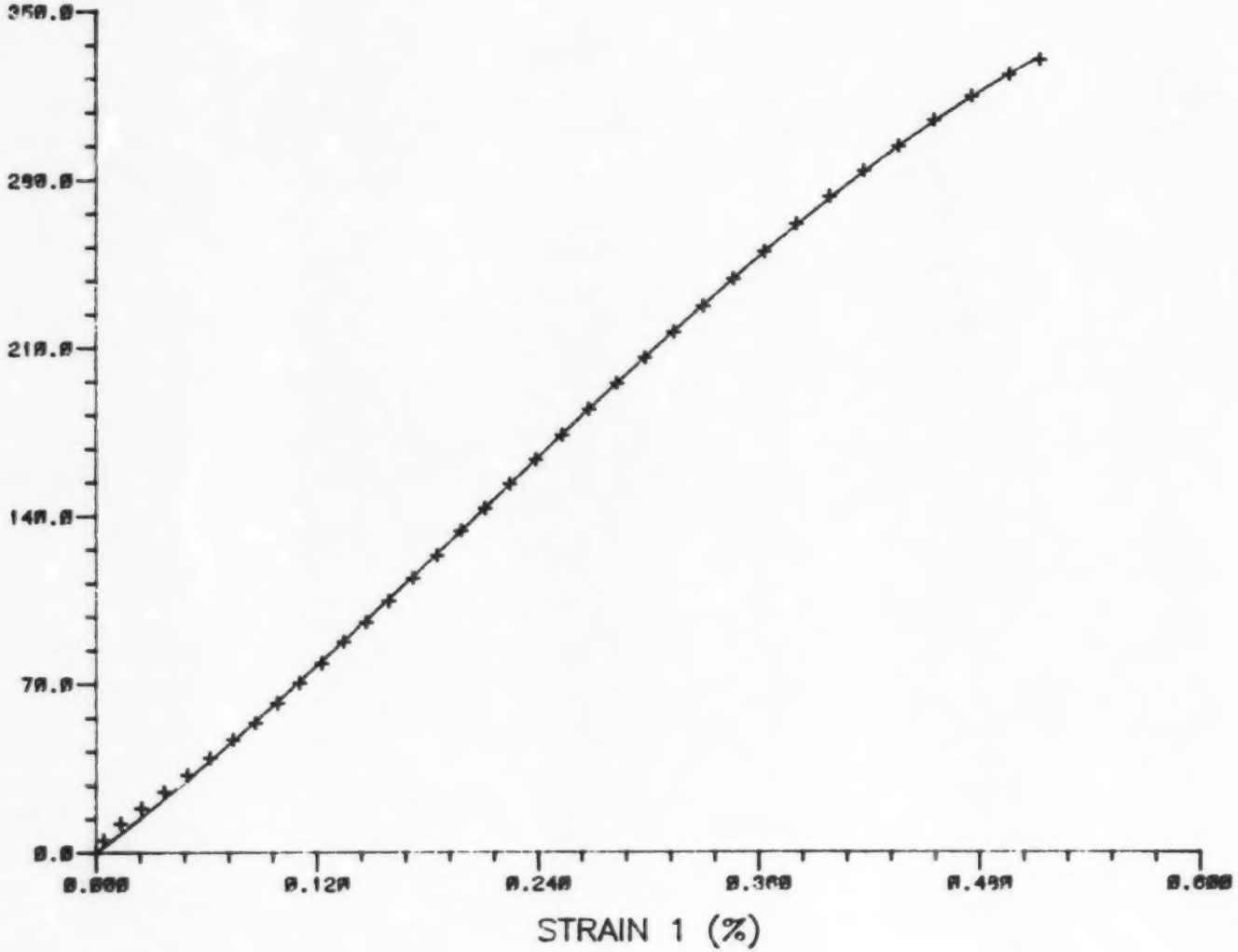

FIG. A26: DEVIATORIAL STRESS VS STRAIN: URL6 226.72 (17.0 MPa)

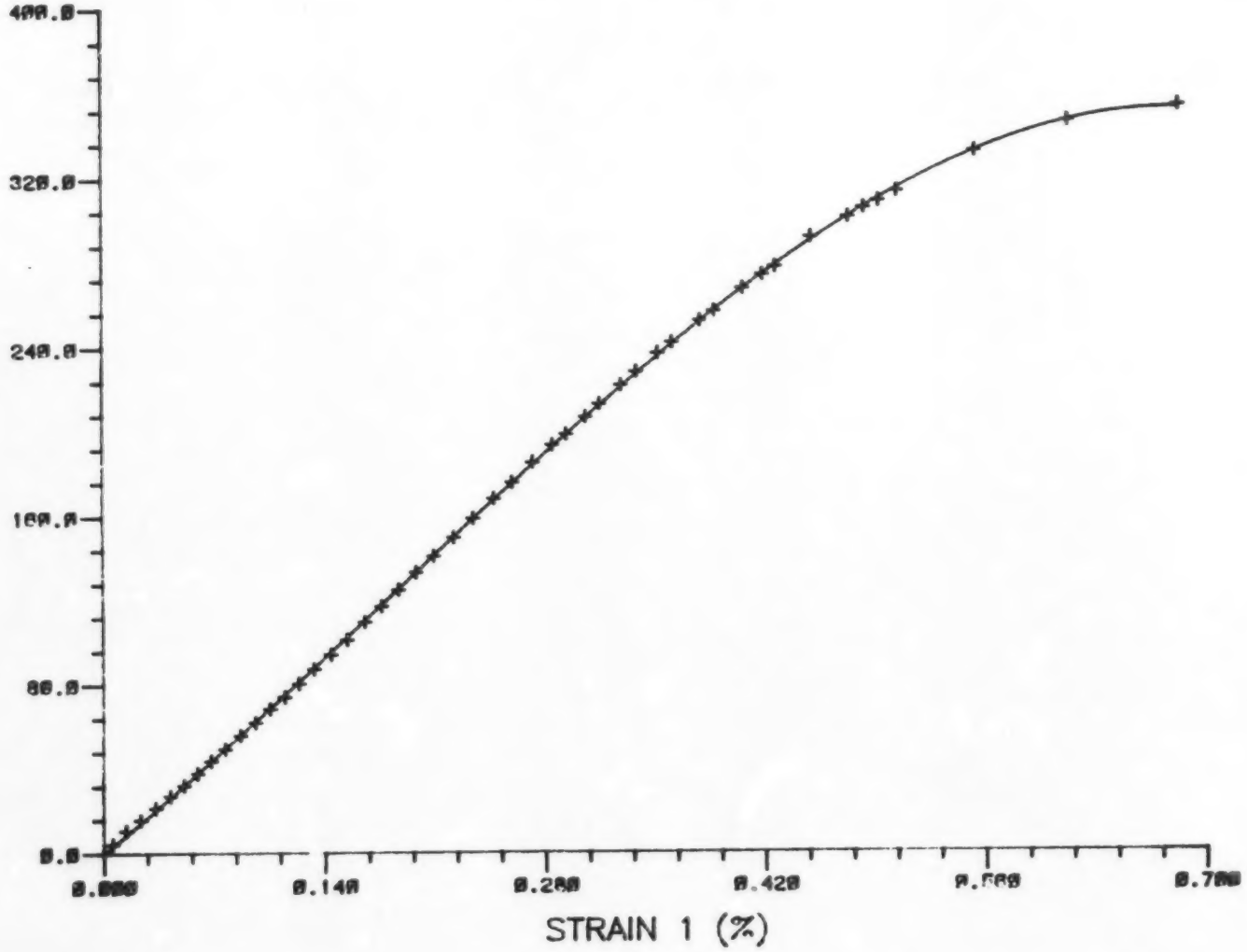

FIG. A27: DEVIATORIAL STRESS VS STRAIN: URL6 259.26 (17.0 MPa)

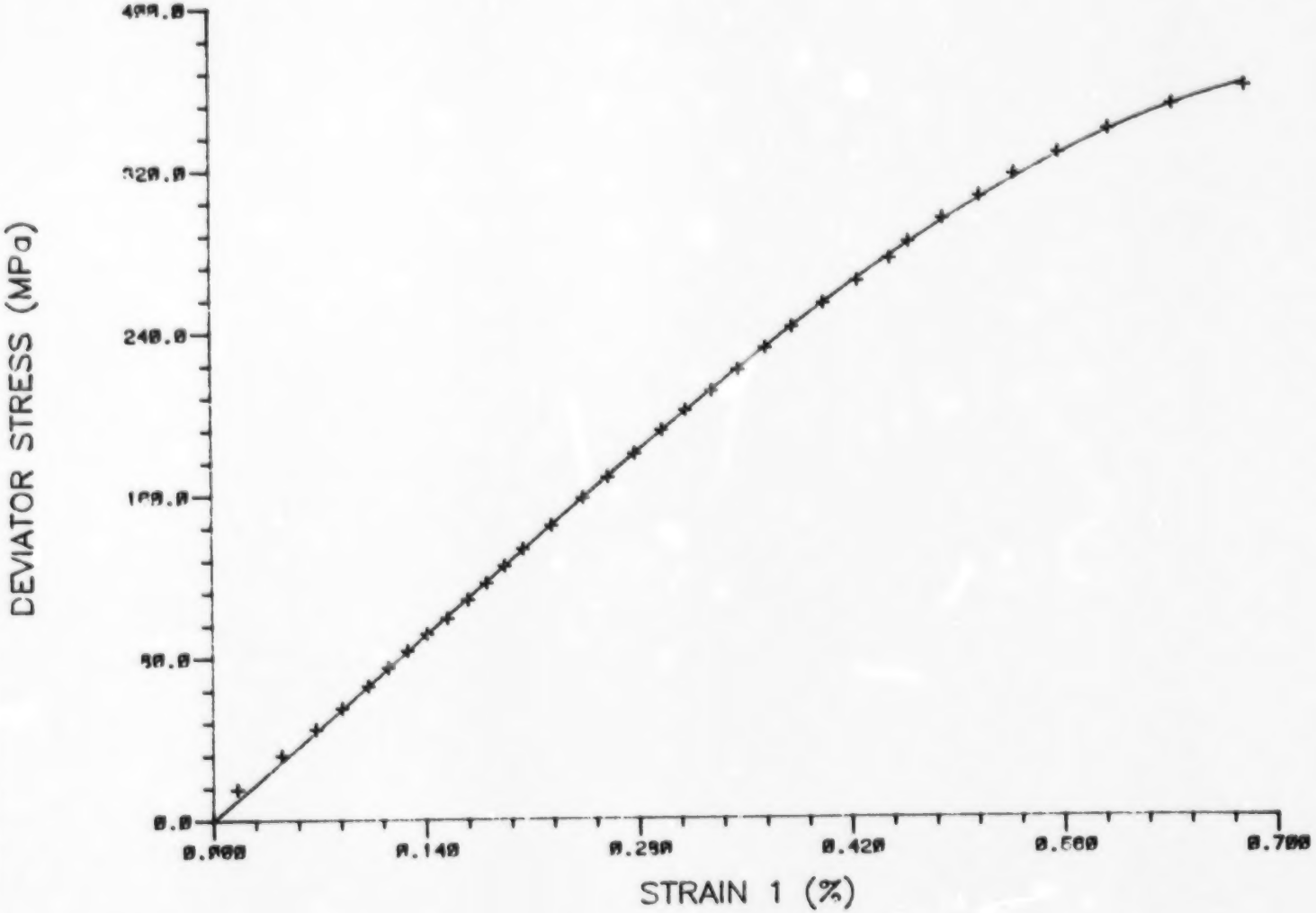

FIG. A28: DEVIATORIAL STRESS VS STRAIN: URL6 227.30 (26.0 MPa)

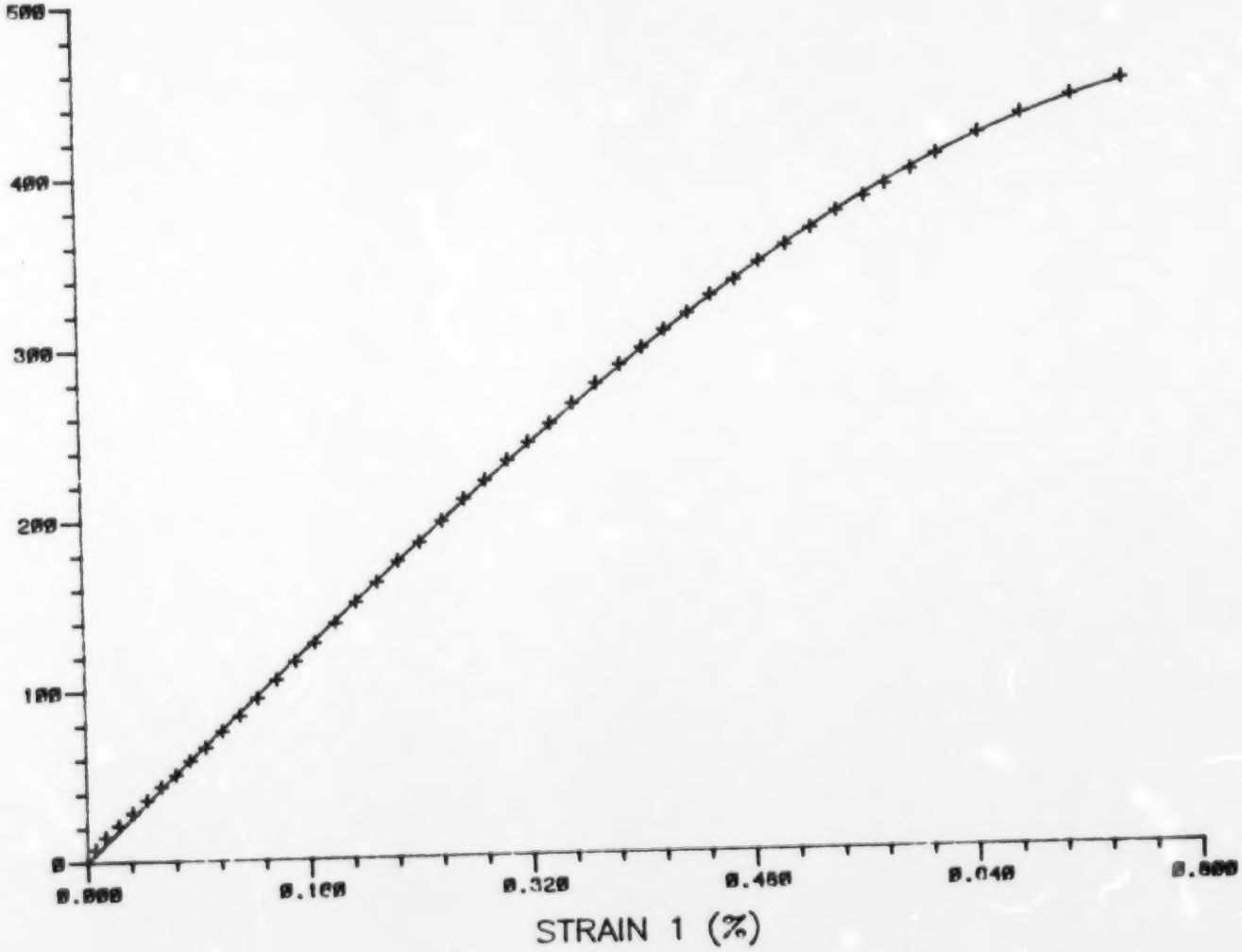

FIG. A29: DEVIATORIAL STRESS VS STRAIN: URL6 228.18 (26.0 MPa)

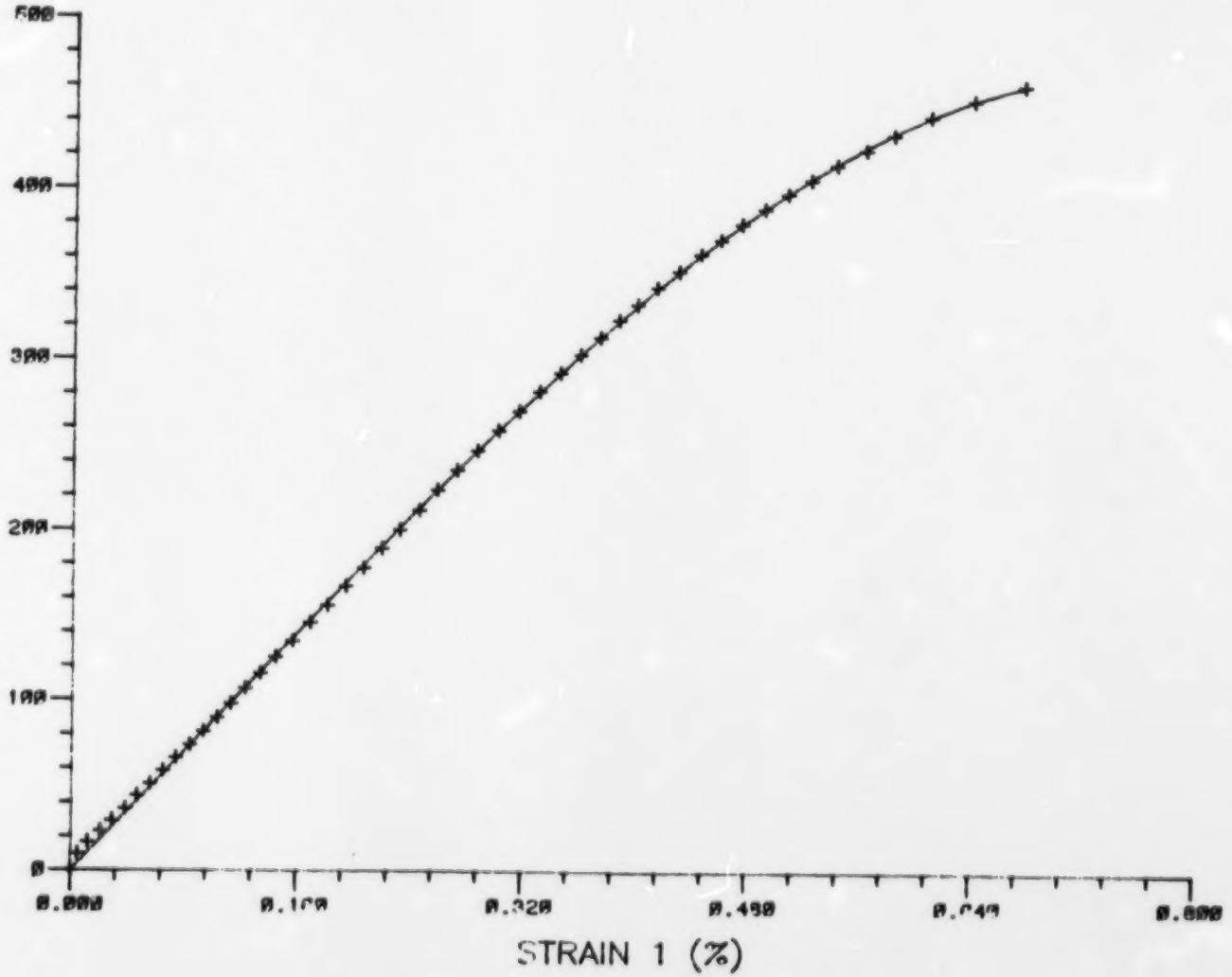

FIG. A30: DEVIATORIAL STRESS VS STRAIN: URL6 225.10 (35.0 MPa)

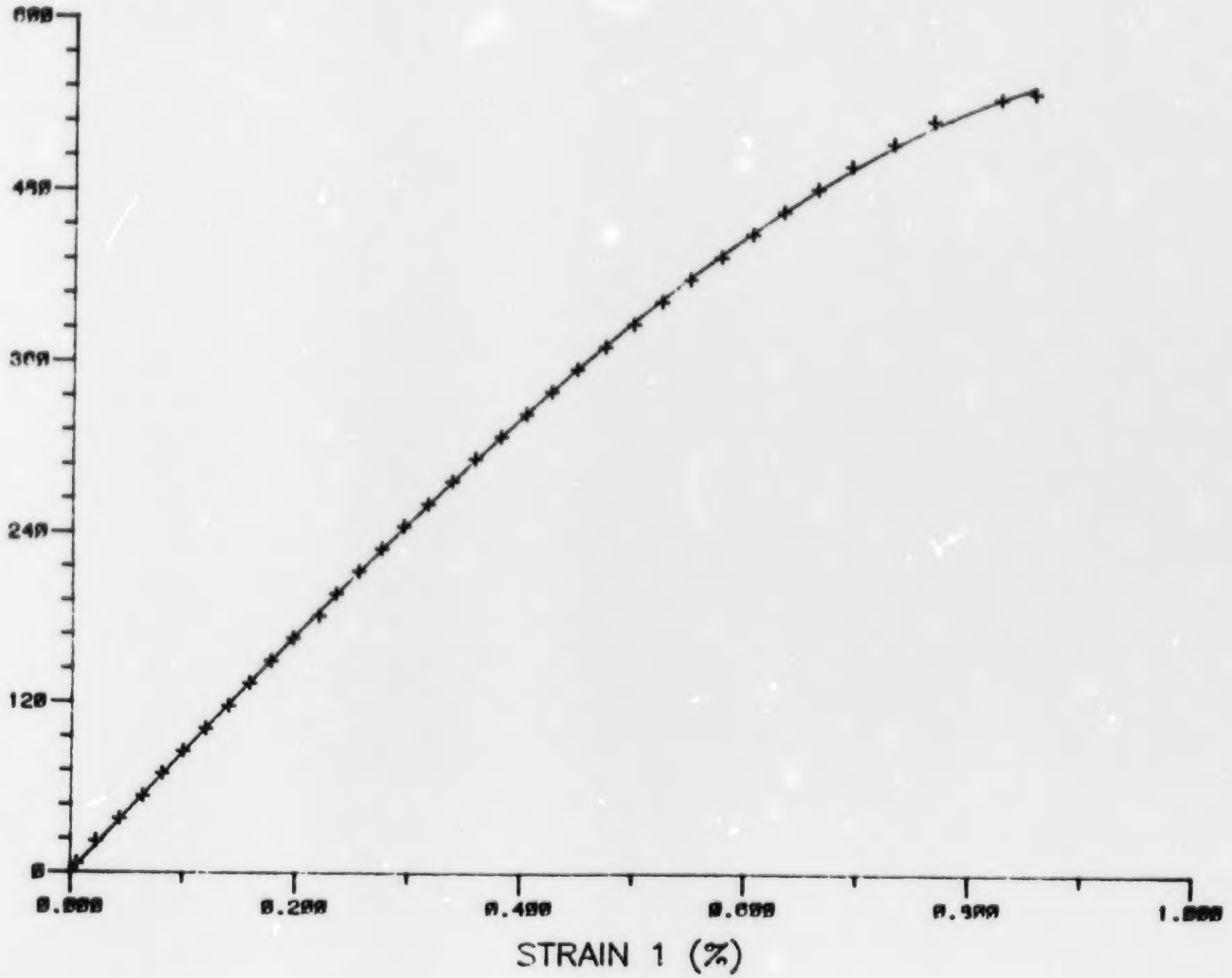

FIG. A31: DEVIATORIAL STRESS VS STRAIN: URL6 226.94 (35.0 MPa)